ALMA MATER STUDIORUM

UNIVERSITY OF BOLOGNA

SCHOOL OF SCIENCE

Laurea Magistrale in Analisi e Gestione dell'Ambiente

Curriculum in Water and Coastal Management

CHARACTERIZING SALTMARSH VEGETATION USING IN SITU OBSERVATIONS AND UAV DATA: A CASE STUDY IN THE VENICE LAGOON

Thesis in: Advanced technologies and decision support systems in water and coastal management

Supervisor

Sonia Silvestri

Presented by:

Ruth Pamela Cuenca Portillo

Co-supervisor

Marco Assiri

Unique session Academic year 2021-2022

ACKNOWLEDGEMENT

My most sincere thanks to my Supervisor Sonia Silvestri and Co-Supervisor Marco Assiri, for your immense patience but most of all thank you for making this work so professional and joyful, thank you for your passion for science and for teaching me so much. I also thank all the NSF project team, for providing me with their data and knowledge as well as for opening their doors to such the prestigious project.

Thanks to all the WACOMA family, especially to professors Elena Fabbri and Irene Laiz for their immense attention and care for me, surely you made this whole process easier. Thanks to my classmates who in these two years have been my family.

Thanks to my friends who are near and far and to my family who believed in me and gave me all their love and support, but above all, thanks for believing in me all the time.

To you dad my angel, from wherever you are, thank you for your strength and for taking me by the hand until the end of this hard journey.

`

ABSTRACT

The geomorphological system, dynamics and spatial distribution of plant species of coastal salt marshes are poorly understood. They are unique systems, which must always grow in height in order to be at peace with the sea level rise. For this reason, the vegetation present as well as the accumulation of organic matter in the marsh accretion process is of utmost importance. There is a lack of information on the spatial distribution with which it is possible to gather information on the existing dynamics in this ecosystem, especially because it has a great variety of species and species associations.

By using the spatial distribution of species, vegetation biomass and in situ observations in a study area, much of these dynamics and functioning can be understood. The present work presents results of data obtained by in situ sampling and data collected by UAVs in the San Felice marsh (Venice lagoon, Italy). The study area hosts at least twelve species of halophytes grouped in six main associations. Samples were collected in September 2021, providing spatially georeferenced data and samples on the distribution of vegetation associations, above- and below-ground biomass, vegetation height, bulk density and soil organic carbon content.

The results suggest (i) the importance of the spatial distribution of the different plant associations as a function of elevation above mean sea level, (ii) the importance of studying the carbon stock capacities in relation to the soil elevation, (iii) a positive correlation between soil elevation and bulk density values. In addition, the results show the importance of studying salt marshes using different sources of information obtained by remote sensing.

`

TABLE OF CONTENTS

`

`

LIST OF FIGURES

`

`

LIST OF TABLES

`

1 INTRODUCTION

The present research is part of a project carried out by the University of Bologna, University of Padua, both in Italy, and Duke University in the United States. This project is called "Coupled ecological-geomorphological response of coastal wetlands to environmental change" and has the following as some of its objectives;

- Objective 1. Field observations of above- and below-ground biomass, Leaf Area Index (LAI), vegetation cover, topographic elevation (also related to the dominant marsh vegetation species), and inorganic matter deposition at the study sites.

- Objective 2 Development, application, and validation of methods to retrieve marsh vegetation above-ground biomass and LAI from LiDAR data.

- Objective 3 Comparison and combination of LiDAR and airborne/satellite Multispectral (MS) information to characterize the distribution of vegetation primary production from the plant to the wetland scale and beyond.

Among the hypotheses of this project is the following; *"LiDAR and MS remote sensing, together with "ground-truthing" field observations can reliably quantify and monitor (repeatedly and cost-effectively) biomass productivity, and hence organic soil production and carbon burial rate, to inform modeling formulations"* and on which the present research is based. All the research will be conducted in two locations to test this hypothesis: North Inlet, South Carolina, and Venice Lagoon, Italy. All field and remote-sensing observations will be collected using aircrafts at North Inlet and have been already collected at the Venice Lagoon using unmanned aerial vehicles (UAVs). North Inlet features very well-studied, extensive tidal marshes (Figure 1), and is the site of a NOAA National Estuarine Research Reserve (Allen et al., 2014), with field research support provided by the 3 Baruch Marine Laboratory (affiliated with the U. of South Carolina). Water properties are regularly monitored, including turbidity. The North Inlet site is characterized by a much higher suspended sediment load than the Venice lagoon, allowing for interesting comparisons between the two systems. Marsh vegetation species at North Inlet include: *Spartina alterniflora* (short and tall forms), *S. patens, S. cynosuroides, Juncus romerianus, Phragmites australis*, *Salicornia spp. and Borrichia spp.,* with the addition of some cattails and sedges in the high marsh adjacent to Winyah Bay (Figure 1).

The Venice Lagoon study site offers contrasting and complementary conditions, including a different set of vegetation species, broadening the range of marsh types providing the empirical foundations for model development. Water properties (including suspended sediments and chlorophyll concentrations) are monitored twice an hour from a network of 10 multi-parametric probes managed by the Venice Water Authority and public data are freely available. Tides and weather data (including wind speed and direction, rain, solar radiation etc.) are also continuously recorded at several stations across the lagoon. Marshes cover a total area of approximately 40 km2 and host at least twenty species of halophytes, among which the most common are *Limonium narbonense, Sarcocornia fruticosa, Spartina maritima, Salicornia veneta, Juncus maritimus, Puccinellia palustris. Phragmites australis* is also present in the inner part of the lagoon, where water is brackish. (NSF Project description, 2019).

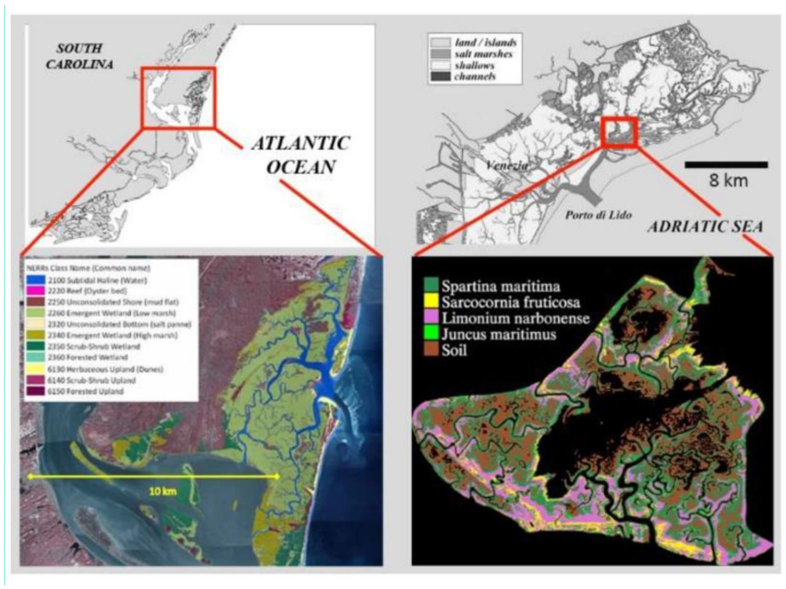

Figure 1 *Study Sites. Left: The North Inlet study site, South Carolina, USA. Water body on lower left: Winyah Bay; on right: Atlantic Ocean. (From Allen et al, 2014; Right: The Venice Lagoon, Italy Source: NSF Project Description, 2019)*

The significance of the project is; that the lack of co-registered information about topographic features, the spatial distribution of vegetation species, and the biomass productivity at the whole-wetland scale is a major obstacle to the development of an understanding of wetland dynamical mechanisms. Remote sensing can change the way we understand wetland dynamics by producing observations of key ecological and biogeochemical parameters over the wide range of scales of interest, from about 1 m to several kilometers. LiDAR remote sensing can provide the necessary canopy characterization, but it has rarely been used for vegetation other than trees (e.g. Yousefi Lalimi et al., 2016a), and even more rarely for marsh vegetation (e.g., see Lefsky et al., 2002).

The project will benefit society by providing tools and data to inform policy and management aimed at preserving and restoring coastal marshes. Specifically, the proposed work will improve our understanding of how watershed and estuarine characteristics influence marsh extent and resilience. The observations and applications

`

are designed to have general implications (with generality bolstered by the application to the Venice lagoon case as well as to North Inlet). The results will be communicated to relevant decision-makers through annual presentations to the North Carolina Water Resources Research Institute, which is attended by decision makers and scientists interested in estuarine conservation. From a societal perspective, the proposed work is important because of the wide presence of wetland systems, both in the US and globally, and the large human populations near the coast that will be affected by responses of coastal wetland landforms to environmental change (NSF Project description, 2019).

1.1 Coastal wetlands

Coastal ecosystems and coastal wetlands in particular, are linked to a very complex chain of inland geomorphological systems. They are supplied by the deposition of sediments, water, and solutes generated by runoff from the interior of the continent. Similarly, there is an exchange of energy, water, sediments, and solutes with downstream marine systems. The complexity of this ecosystem is the result of these processes, as it depends on many factors to find its balance and function properly. This balance can be disturbed by small changes in the surface systems of the Earth. For this reason, it can be said that coastal wetlands are a very sensitive eco-geomorphological system. They are overly exposed to environmental changes and global warming and with these imbalances they suffer the direct consequences on the amount of sediment transported to them, the intensity of subsidence and the amount of nutrient concentration (e.g., Kirwan and Murray, 2007).

Many of these processes and values have changed over time, due to changes that humans have made to the environment. For example, the construction of dams has reduced the transport of sediment to coasts worldwide (Syvitski *et al.,* 2005), resulting in a deficit of sediment in coasts, making it impossible for them to naturally counterbalance sea level rise and erosion (Kirwan *et al*., 2010). Anthropogenic pressures have increased significantly in coastal areas and will continue to increase as half of the world's population lives within 100 km of the coast (Bagarrán *et al*., 2015), with a very high probability that these pressures will continue to increase over time. This has led to widespread land-use changes in coastal areas and, consequently, the loss of 50% of coastal wetlands in the 20th century (UN WWAP, 2003).

Because they are transitional ecosystems in which biotic and abiotic processes are equally important in controlling dynamics, coastal wetlands provide a variety of ecosystem services, the most important of which are flood control, nutrient cycling, coastal disturbance control, and greenhouse gas and climate control (Temmerman *et*

`

al., 2013). Coastal wetlands play an extremely important role in the carbon cycle and their total area worldwide is disproportionate to their importance, which has only recently begun to be quantified (Chmura et al., 2003, Pendleton et al., 2012, Holmquist *et al.,* 2018). In fact, carbon storage per unit area in a coastal wetland can be three times higher than in a tropical forest (Pendleton *et al.,* 2012), and the rate of carbon burring per unit area is higher in a coastal wetland than in any other biome, about 30 to 50 times higher than in a forest (McLeod *et al.* 2011).

1.2 Halophytes species

Halophytes are plants that can adapt to life in saline environments, most of which are angiosperms. For their survival, halophytes require osmotic adaptations achieved by the ions in their environment. At the cellular level, these plants depend directly on their ability to accumulate ions, allowing them to grow even in the presence of water deficit and ion deficiency. Much research is still being done on these peculiar. Studying the production and functioning of these plants from an agricultural point of view is crucial and forward-looking, since most of the water on our planet is salty. (Flowers *et al.,* 2010).

Salt marshes can be defined as *halophytic grassland* in sediments adjacent to salt water, whose water level changes as the tidal forcing (Biftink, 1977). A central part of identifying salt marshes is the introduction of halophytes, which are salt-tolerant plants that can complete their entire life cycle in saline environments, as opposed to glycophytes that grow in non-saline habitats (Flowers, 1975; Flower et al., 1986; Jennings, 1968). Coastal salt marshes are located on the border between land and sea, and their origin and survival depend largely on eustatism and the subtle balance between erosion and subsidence. The formation of interglacial salt marshes is usually explained by an increase in the rate of mud deposition, an increase in ground level and rare flooding of the bedrock, which can be colonized by new root crops (Petik, 1984; Allen, 2000; Friedrich and Perry, 2001). After the formation of plants, plant debris accumulates, sedimentation of inorganic sediments increases, and the surface of the marsh is fixed to the roots of plants.

Interestingly, the salinity tolerance characteristic of halophytes does not necessarily imply the need for a saline environment. Some species are actually essential halophytes, i.e. plants that require a saline environment (e.g., Adam, 1990), while most others thrive in environments without salinity. In addition, there is no general agreement on the salinity limit that distinguishes halophytes and glycophytes, in part because of the high variability of salinity resistance in soil water (Adam, 1990). Interestingly, despite their ability to grow in non-saline environments, halophytes are found only in saltwater

`

habitats. This limitation of the presence of salts is due to competition with glycophytes that are better adapted to salt-free environments (Riley *et. al.,* 1970).

The spatial distribution of halophytes in salt marshes is not random but organized in patches (Silvestri et al., 2004), when visiting one, is easy to identify those patches, as seen in Figure 2 and this increase the interest in the study of plant zonation. Some authors (e.g. Chapman, 1974) described plant zonation in salt marshes and evaluated the relative importance of different environmental factors in determining halophyte zonation.

Figure 2 Example of a patch on San Felice salt marsh

Some early hypotheses zoning related to the concept of "succession", is based on the assumption that sediments remain on salt marsh plants (Silvestri et al., 2004), where the substrate becomes more stable after the initial colonization phase. This allows other species to invade the marsh and initiate changes targeting mature and sustainable climax ecosystems (Odum, 1971). According to this model, when soil height increases and sufficient sediment is provided, the growth of the marsh is balanced by subsidence (Allen, 2000).

1.3 Saltmarsh soils organic matter, sediments

Salt marshes grow mainly on fine sediments, while salt plants grow on sand and sometimes on gravel soils. In salt marshes, both roots and invertebrate fungi affect soil structure and create macropores in the soil. Invertebrates also cause bioturbation where sediments can float and erode. This effect can be neutralized by algae and other microorganisms that form biofilms stabilize the soil surface. The biofilm cements soil

`

particles and reduces erosion. It also adds organic matter and the algae with cyanobacteria fix nitrogen. Due to the high organic content and high moisture of the microbes in wet areas with brine, the amount of oxygen is often slightly below the surface level. This is especially true in lower intertidal areas and impounded marshes. Salt marshes are usually rich in sulfur-forming sulfides, which darken the soil, give off the characteristic odor of rotten eggs, and stress many plants. In intermittent regions, soil microbes, sulfides, and flooding regimes often reduce the abundance of flood-prone species to uniquely resistant species (Zedler, *et. al.,*2018).

The presence of oxygen is determined by the frequency and duration of marsh floods, which determines the physiological needs affecting aerobic respiration of roots, plant development and soil aeration, which affects the germination and early growth of seedlings (Chapman, 1964). Salt marsh vegetation has adopted a variety of strategies to survive the periodic saturation of the soil. The first strategy is the formation of aerenchyma, a network of intercellular porous spaces that distribute air from vascular tissue, allowing it to breathe even when the soil is saturated (Wisser et al., 2000). Although the formation of aerenchyma can be stimulated by low oxygen partial pressures and floods, there are significant differences in the ability of species to develop aerenchyma, for example *Halimion portulacoids* is specie that cannot develop aerenchyma, while *Spartina alterniflora* has very wide aerenchyma (Armstrong, 1982). It is important to note that even in species with large non-substances, access to oxygen through this process is limited, providing aerobic respiration only in relatively short periods of flooding. Another strategy for long-term flood survival is to increase the pore size of surface tissue. In fact, non-swamp plants are characterized by low tissue porosity (2-7% by volume), and this stomata volume will be insufficient to ensure adequate oxygen diffusion of roots at flood. The wetland porous spaces can occupy up to 60% of the plant's body (Armstrong, 1982).

1.4 Light Detection and Ranging (LiDAR)

Laser scanning is practically defined as a system for creating digital surface models. The main component of this system consists of a set of sensors, recording devices and various programs, the result of these processes, most of the time, is a LiDAR point cloud stored in LAS format. A laser device measures a distance called "laser range", when a laser rangefinder is installed in an aircraft, it measures the position and proximity of the aircraft by measuring distances corrected by GPS and Inertial Measurement Unit (IMU) that allows a GPS receiver to work when GPS-signals are unavailable and helps to determine the ground pattern (X, Y, Z) by following the polar measurement principle of coordinates, shown on Figure 3, so we can define the coordinate system and say that Z means altitude. The high values produced by the

`
laser scanning of the aircraft do not refer to the height of the "ground points" as a model of the actual digital height, since the results give us an idea of what height the sensor "sees". Post-processing is required to obtain a digital terrain model (DTM) from a digital surface model (DSM). (Kerle *et al.,* 2004).

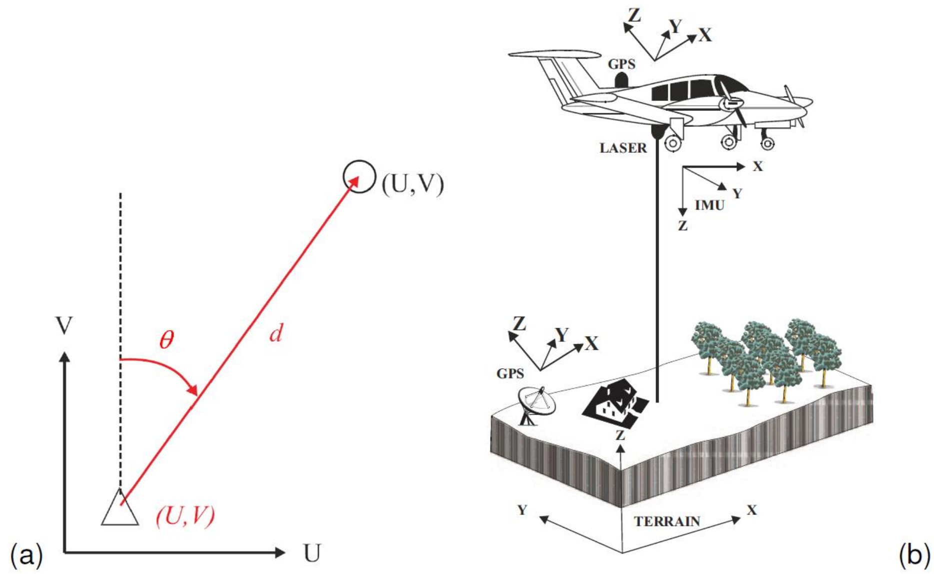

Figure 3 *Polar measuring principle (a) and its application to ALS (b) (Source: Principles of remote sensing book, Kerle et al., 2004)*

The main features of airborne laser scanning (ALS) are: high-precision, high-resolution DTM with little or no dependence on weather, season, and lighting conditions. A laser is the amplification of light by forced radiation. The laser emits a monochromatic beam of light in the near infrared spectrum (NIR). The radiation is not really a single wavelength, but has a spectral band of less than 10 nm. It is determined that the laser emits the highest intensity of radiation. Most airborne laser devices are "pulsed lasers", a pulse is a very short signal that propagates in the form of a beam. When a pulse is sent, the timer starts and stops when it returns, the elapsed time is measured with a resolution of 0.1 ns, since the speed of light is a constant, the distance can be easily calculated. Modern laser scanners emit pulses at very high frequency (up to 250,000 pulses per second). A complete scan is usually done by moving the mirror that deflects the laser beam. Simple laser rangefinders record an inverse pulse for each pulse emitted. Modern airborne laser rangefinders record multiple echoes of a single pulse. A Multiple return laser ranging is specifically relevant for flying terrain with vegetation, because it helps distinguish plant echoes from ground echoes. Points are generally classified depending on their height, points with a lower z-value will generally be classified as ground points and the others, depending on their characteristics, will have different classifications. A multi-point survey does not provide a direct answer about what this point represents, but it helps to find it. (Kerle *et al.,* 2004).

ALS provides three-dimensional coordinates of ground points. To calculate the exact coordinates of the ground, we must carefully consider all the necessary elements. The distance from the aircraft to the ground can be measured in centimeters with the greatest accuracy using a laser rangefinder. Using dual-frequency receivers, we can accurately determine the position of the aircraft using another GPS. We use the IMU, to accurately determine the location of an aircraft when measuring distance. After the flight, the recording and the position and orientation system of the laser device (i.e., the integrated GPS and IMU) are recorded simultaneously and used to produce the points (X, Y, Z coordinates). The resulting product may contain system errors and is often referred to as "raw data". Further data processing should solve the problem of extracting information from ambiguous coordinates (X, Y, Z). (Kerle *et al.,* 2004).

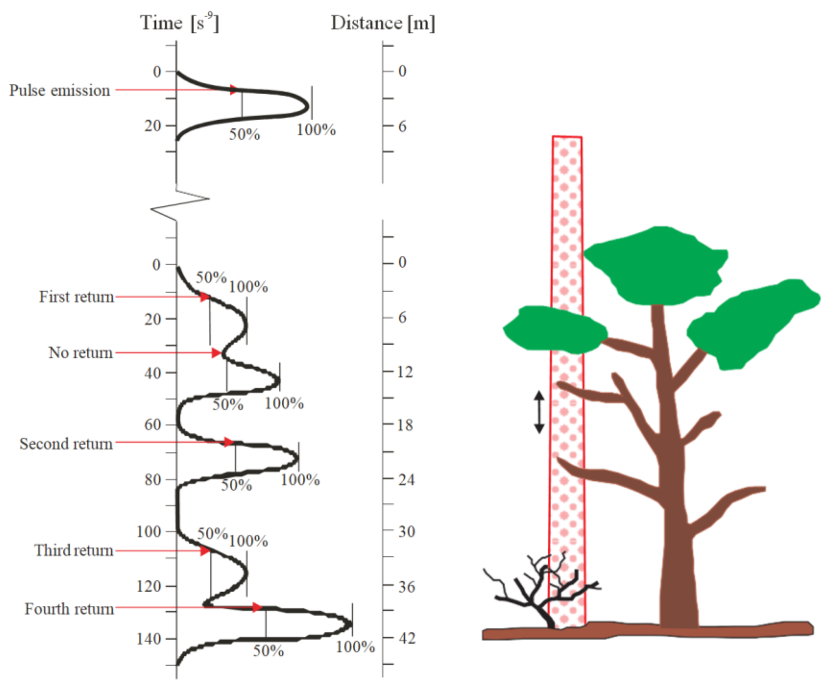

Figure 4 *Multiple return laser ranging (Source: Principles of remote sensing book, Kerle et al., 2004)*

Proper computer calibration, accurate flight planning and execution (including logistics of GPS), and the right software are important to obtain accurate information at the right time. ALS produces a DSM that is directly comparable to the imagery obtained from aerial photographs / orthophotos.

`

1.4.1 Storage and classification of LiDAR Data

The most common form of storage of a LiDAR point cloud is the .las format, this format was developed by the American Society for Photogrammetry and Remote Sensing (ASPRS); stores LiDAR and is used to exchange LiDAR data between data providers and data consumers. The latest version of the LAS format specifications is version 1.4, approved in November 2011 and published by the American Society for Photogrammetry & Remote Sensing. For point classification (ground, water, vegetation, buildings, power lines), he concept is similar to the supervised and unsupervised classification of satellite imagery. However, for LIDAR, classification is based on the geometric position of the return relative to its neighbors and the category of the first/last return (if there are multiple returns for a single pulse, only the last one may be on the ground). Classification can be a processing-intensive operation, and many LIDAR are provided with limited classification. Ground is almost always included in a LAS file because it is needed to create a DTM. The commonly used versions of the LAS format (1.2 and 1.3) approved by the Board in February 2008. They have 8 predefined classification categories and can process up to 32 (shown in Table 1). The newer version (1.4) has about 20 predefined classes and can process 256 categories.

ASPRS Standard LIDAR Point Classes

Classification Value (bits 0:4)	***Meaning***
0	**Created, never classified**
1	**Unclassified[1]**
2	**Ground**
3	**Low Vegetation**
4	**Medium Vegetation**
5	**High Vegetation**
6	**Building**
7	**Low Point (noise)**
8	**Model Key-point (mass point)**
9	**Water**
10	***Reserved for ASPRS Definition***
11	***Reserved for ASPRS Definition***
12	**Overlap Points[2]**
13-31	***Reserved for ASPRS Definition***

Table 1 *1.2 ASPRS Standard LiDAR Point Classes (Sourse: LAS format specifications for ver. 1.2)*

1.5 Digital Surface Model (DSM) and Structure for motion technique

A DSM captures a surface, including natural and human-made structures such as vegetation and buildings. They illustrate the reflective surfaces of all features located

`

above the "bare earth." In short, DSMs represent the Earth's surface and all objects on it. DSMs can be efficiently created by automated image matching of high-resolution optical stereo images or by stereophotogrammetry. Stereo matching of images is used to find corresponding pixels in image pairs, which allows 3D reconstruction by triangulation when both the outer and inner orientations are known.

Structure from Motion (SfM) photogrammetry is a method for approximating a three-dimensional structure using two-dimensional images. The photos are stitched together using photogrammetry software to create the three-dimensional (3D) model and other products such as photomosaic maps. Photogrammetry involves taking images with unmanned aerial vehicles (UAVs) or remotely operated vehicles (ROVs). A camera moves over the site on a pre-planned route and takes hundreds or thousands of photos from above, the sides, and the interior of the structure. It is important that the photos overlap so that every inch of the site is captured from multiple distances and angles.
Once the divers or UAVs have finished capturing images, the photos are merged into one large file and corrected for color balance and exposure. The images are then processed using photogrammetry software. The program uses an algorithm to create a photo mosaic that retains the details of each image, and then looks for common landmarks in the photos, such as a ship hull fragment. Each landmark is aligned using data about its size, area, and spatial position in the landscape; all this information is used to create what is called a data point cloud. This point cloud is used to map nodes or vertices onto a solid surface, creating a 3D model of the site. At this point, the model is completely colorless, so the software uses color data from the original images to "paint in" the pixels of each feature.

The workflow of SfM photogrammetry can be summarized as follows (e.g., James and Robson, 2012): the first stage features are defined in each image and matched between overlapping frames (e.g., Lowe, 2004), using the Scale Invariant Feature Transform algorithm. The second stage is to reconstruct the geometry of the image lines with repeated ray correspondences (e.g., Snaveli *et al*., 2006). At this stage, there is an internal configuration of the space that describes the interior, camera geometry (focal length and base point and additional distortion parameters); external parameters, including position (3 displacements) and orientation (3 displacements) and the rotation in which the image was captured. Also, the coordinates of the 3D object is calculated from the coordinates of the 2D image in any coordinate system. Homologous image points rarely produce point clouds. With knowledge of painting line geometry, including the calculation of whether a dense point cloud can be obtained it looks more closely at almost every pixel of the image corresponding to a 3D point according to the algorithm (Remondino *et al*. 2014). With the resulting 3D point cloud during installation, a geolink

`

can be created and take into account additional information by optimizing the internal and external settings of the camera or by analogy later; this change leaves no room for improvement. Advances in algorithms and software enable the easy use of SfM photogrammetry and basic elements of photogrammetry can be easily used for land reconstruction. Principles are still needed to reliably assess accuracy (e.g., Carbonneau Dietrich, 2017) in the 3D model and to avoid possible deviations that could lead to misinterpretation. The use of ground control points is of crucial importance for good product quality.

1.6 Scope of the research

The main objective of this research, as mentioned in the title, is to analyze the vegetation in a coastal wetland in the Venice Lagoon, Italy. For this purpose, samples of different species were collected and processed in the laboratory, representing the first source of information. The second and the third sources of information were obtained using UAVs that provided data by, orthophotos and a LiDAR point cloud.

The comparison of the three sources of information will allow us to understand to what scale and with what accuracy it is possible to analyze ecosystems of this type, which have very particular characteristics and are very vulnerable. Any study or sampling that is done in this place affects them very aggressively. So we can say that the first and most important objective is to develop a methodology for remote data analysis to study coastal wetlands without affecting them, using the technology associated with the geographic information systems (GIS) and remote sensing.

The final objective planned for the present study understand if we can retrieve the LAI of the different plant associations present at the site using LiDAR data and compare with the calculations made as a result of *in situ* sampling.

2 METHODS

2.1 Study Area – The San Felice Salt Marsh (Venice Lagoon, Italy)

The study area is located in the Venice Lagoon NE Italy (Figure 5), which is connected to the Adriatic Sea by three inlets, Lido, Malamocco and Chioggia. The Venice Lagoon has an area of about 550 m^2 with an average depth of approximately 1.1 m and characterized by a semidiurnal tide with a range of about 1.4 m (Belluco *et al.,* 2006). The average volume of water in the lagoon is about $700x10^6$ m^3, the half-day volume

`

exchange with the sea is about $350x10^6$ m^3 during the spring tides and $175x10^6$ m^3 on the neap tides (Silvestri *et al.,* 2000).

The present study focuses on the San Felice salt marsh and it's characterized by relatively healthy vegetation conditions and is colonized by halophytic vegetation associations dominated by the following species: *Salicornia veneta* (hereafter "Salicornia"), *Spartina maritima* (hereafter "Spartina"), *Limonium narbonense* (hereafter "Limonium"), *Sarcocornia fruticosa* (hereafter "Sarcocornia") and *Juncus maritimus* (hereafter "Juncus"), *Inula crithmoides* (hereafter "Inula") (Belluco *et al.,* 2006.,Silvestri *et al.,* 2005, Wang *et al*., 2007, Silvestri *et al.,* 2002, Yang *et al.,* 2020). In the present study, the presence of *Spartina anglica* (hereafter "Spartina Anglica"), an invasive species extensively distributed in the study area, was detected by field observations. This species was not mentioned in previous studies conducted in the same area. Previous studies of the spatial distribution of these species over the San Felice marsh has been done, form a small spatial scale and *in situ* measurementes by Silvestri *et al.,* 2003 and by the use of remote sensing extending the analysis for the whole marsh by Belluco *et al.,*2006; Marani *et al.,* 2006, Wang *et al.,* 2007; and Yang *et al.,* 2020. The surface of the San Felice marsh has decreased in the last century, mainly due to the formation and expansion of internal ponds and lateral erosion from wave attack (Day *et al.,* 1998).

The fresh water of the streams is rich in nutrients and many pesticides, but the sediments transported are very small, so there is no significant change in the load on the sediments during periods of growth or flooding. Importing 7,000 tons of nitrogen and 1,500 tons of phosphorus per year, the lagoon can be considered a eutrophic environment. Historically, human activity has greatly influenced the shape of the lagoon. In the 15th and 16th centuries, the three main rivers that flow into the lagoon turned directly into the sea. A deep canal was dug in three bays and a long reservoir was built. Currently, there are few areas in the lagoon that have not been affected by human intervention; especially the southern and central parts of the lagoon are affected by heavy erosion. The study site is characterized by modest sediment imputs from two small rivers and from the sea, the soil elevation range lies between 10 and 50 cm above mean sea level (m.s.l.) (Silvestri et al., 2005).

`

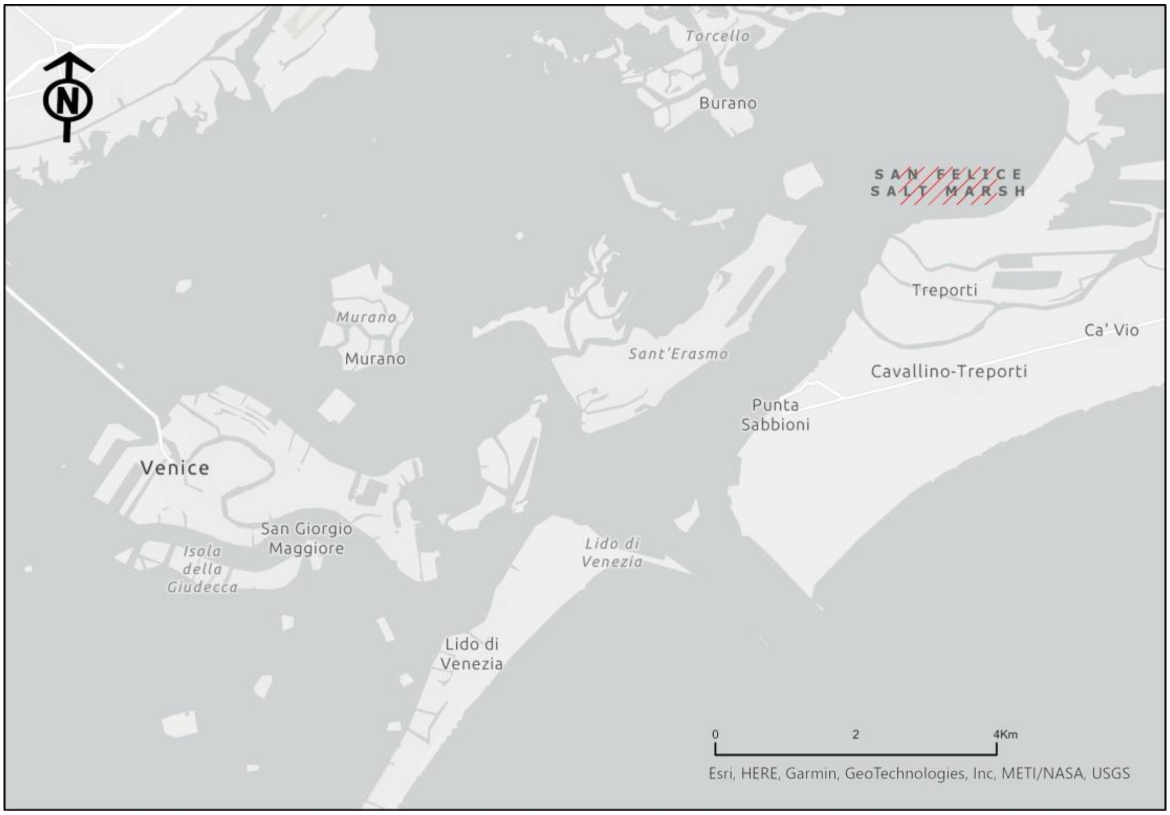

Figure 5 Location of the San Felice salt marsh inside the Venice Lagoon

2.2 Field campaign

Thirty-two hectares of San Felice marsh were overflown with UAV systems carrying different sensors by a survey company called Archetipo. Several overflights were performed, and the products obtained were Hyperspectral images, LiDAR point cloud, Orthophoto, and a DSM derived applying the SfM processing to the orthophotos. In this work we analyze LiDAR data as well as the DSM.

The team consisted of two people in charge of the drone survey, who set up a base on a flat spot in the marsh from which they flew, and four other people in charge of going around the marsh to take samples and perform various tasks. The first work consisted of placing 28 square targets of 50x50 cm; they were located using a GPS and designated as ground control points, the distribution is shown in Figure 6. All the work had to be done very quickly, because in this ecosystem we had only half a day, because if we walked during high tide, we would risk damaging the ecosystem much.

Figure 6 Map of the sampling area showing the location of the points where the ground control points targets were placed and the photo of the moment when one of the targets was located

To avoid our presence at high tide, the work started very early, around 5:30 in the morning, and lasted until 15:00, times when the tides were low at this time of year as seen on Figure 7. After the entire drone overflight was completed, all targets were removed. Sampling was conducted during the week of September 5-11, 2021.

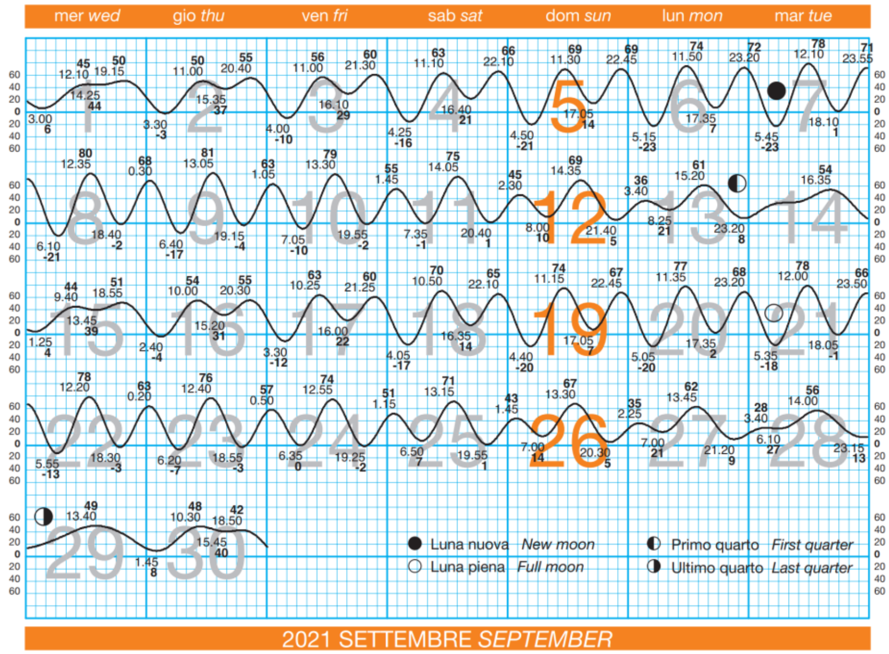

Figure 7 Tide on the study site in September 2021 (Source: Astronomical tide prediction in Venice,2021 Centro Previsioni e Segnalazioni Maree Città di Venezia)

After the target placement and collection work was completed, we began to collect the vegetation and sediment samples. A total of 10 plots were selected, in each of them three replicates called bio were performed. With the support of a Leica GPS/GNSS system, all sampling points were accurately located, as shown in Figure 8. GPS data were also collected randomly in order to collect as much data as possible, taking advantage of our presence in the study site, which due to its location, is not very easy to reach.

Figure 8 Location of the 10 plots inside the study area

Prior to the trip to the work site, team meetings were held in order to organize the materials and roles to be taken into account in the field. It is very important that all the work is extremely organized and that each person occupies his or her role so that all the information collected is correctly organized and nothing is lost. Teamwork is crucial for a good result. It is also important that the methodology of the subsequent analysis of the collected data is correctly determined, as the sampling methodology, sample quantities, organization and distribution of sites, among other details that cannot be decided only in the field, depend on it. The list of materials used is presented in appendix 6.1.

When the samples were taken, the work was organized as follows: two people were responsible for collecting the samples, both vegetation and sediment samples, the other for organizing the samples in plastic bags, labeling the bags by plot and bio, and noting the observations that could be made in each case and taking detailed photographs of the process. The correct noting of data, observations and photos is crucial so that everything can be done correctly later in the laboratory and to have a point of contact for clarification in case of discrepancies.

`

The parameters for selecting the sampling sites or plots were: good presence of the main halophyte species of the area, best representation of plant associations and best possible representation of high, medium and low zone species. The sampling procedure was to collect three types of samples for three different kinds of laboratory analyzes:

1. Vegetation analysis – aboveground biomass
2. Vegetation analysis – belowground biomass
3. Soil bulk density analysis and organic carbon though loss of ignition (LOI) analysis

The first step was to choose a suitable and meaningful location for the surrounding vegetation. Two rulers forming a square were placed on the ground to form an area 1 meter by 1 meter. The coordinates of the 4 angles and the center of the square were determined. Then the heights of the vegetation at the 4 corners as well as in the center were measured as seen in Figure 9.

Figure 9 Sampling area scheme, the red dots represent the places where GPS points where taken and the red lines the places where vegetation height were measured

After delineating the area to be sampled, observations of the plot were noted and an estimate of the percent occurrence of each species within the delineated area was made, and a photograph of the plot was taken. The person in charge of this work had to pay very close attention to detail and carefully make the notes and observations on each plot. The data collected of each plot have been organized in tables, as shown by the example of plot 1 in Table 2. The remaining observations for the other plots can be found in appendix 6.2.

`

Estimation of Vegetation Cover – Plot 1	
Cover	**Percentage (%)**
Limonium	80
Sarcocornia	10
Soil	10

Vegetation Height (cm) – Plot 1	
Corner 1	21
Corner 2	20
Corner 3	6
Corner 4	7
Center	10

Plot 1 - Picture


Table 2 Demonstration of how field observations were organized after data collection was completed

Once the observations in each plot were performed, we proceeded to the actual sampling. The first sample, bio 1, was taken in the exact center of the delineated and observed area. The two repetitions, bio 2 and bio 3, were randomly selected by casting the 20x20 cm quadrant no more than 3 m from the center.

2.2.1 Vegetation Sampling

For each bio, the surface vegetation of the sampling area was completely removed, taking special care not to remove any roots, since the goal in this case is to represent aboveground vegetation. Knives and scissors were used to cut off the vegetation and then all of the collected material was placed in plastic bags. Each bag was immediately identified with the corresponding plot and bio. Figure 10 shows an example of how bio 1 was arranged in relation to the plot and what the area looked like after all the vegetation was collected.

An additional 25 vegetation samples were collected to spread the sampling a bit further into the marsh. These samples were also collected to improve the representation of species represented in the salt marsh. Therefore, a total of 55 vegetation aboveground samples were collected and processed.

Figure 10 Vegetation sampling and demonstration of the area known as bio

2.2.2 Sediment sampling

Once the vegetation was completely removed, we proceeded to soil collection. For this purpose, we divided the area into 4 small squares of 10x10 cm. The first quadrat was used to collect soil samples to be used for soil bulk density and organic carbon analysis by loss on ignition (LOI) analysis. For this purpose, we used a core with a diameter of 10 cm and a depth of 10 cm to obtain a constant volume for all samples. Once the samples were collected, they were placed in plastic bags and labeled.

`

Figure 11 Soil and below ground sampling area and different cores used for each

For the next step, i.e. the soil samples to be used for the belowground dry biomass analysis, we used another 10x10 cm square that had been least disturbed during the previous sampling. In this case, on the first day of work, we used the same core with a diameter of 10 cm and a depth of 10 cm. However, on the following days we decided to increase the depth of the sample, i.e. we used a core of 30 cm depth and 8 cm diameter (see difference in Figure 11). In this case, after sampling and before storing the samples in plastic bags, we cut the sample into 3 pieces of 10 cm length, as shown in Figure 12. The first piece corresponds to the most superficial, designated as "first part" at a depth of 0-10 cm, "second part" at a depth of 10-20 cm and "third part" at a depth of 20-30 cm. Each piece was then kept in plastic bags and labeled with plot, bio and the corresponding part of the sample. The results obtained will be discussed and shown in the next chapter.

`

Figure 12 Belowground samples cut into 3 pieces on 10 cm each

In order to preserve the properties of the samples and protect them from heat, they were kept in thermal bags during sampling.

2.3 Transportation and Preprocessing

After each day, the vegetation samples were weighed to obtain their wet weight, put in paper bags (Figure 13) and then dried in the sun. All paper bags were carefully identified. The bags were weighed without introducing vegetation samples and after introducing vegetation. They were then transported to the lab for further desiccation in the oven. Soil samples (i.e. for LOI and belowground vegetation determination) were frozen until the day they were processed in the laboratory.

2.4 Laboratory analyses

All laboratory analyses were performed at the laboratories of the University of Bologna, Faculty of Environmental Sciences, Via Sant'Alberto, 163 in Ravenna.

2.4.1 Vegetation analysis for aboveground dry biomass (g/m^2)

Paper bags with vegetation samples were placed in an oven at 70°C for 72 hours to remove the humidity present in the samples. Whenever possible, the weights were recorded twice a day to ensure that the samples were stable in weight before they were taken out of the oven. After the samples were removed from the oven, the bags were weighed first with vegetation and then without vegetation to determine exactly how much the vegetation alone weighed in a dry and anhydrous state. A table was prepared with all the notes related to weight and is presented in appendix 6.4. In the table results corresponding to the 10 plots can be seen, each plot with its three replicates, as well as 25 other samples collected in the area. A total of 55 collected samples were analyzed. The results were obtained in a total of 72 hours; all samples have reached weight stability in that time. Weight control was carried out periodically, approximately twice a day, in order to know when the samples reached a stable weight. All of this information and accurate knowledge of the sampling area, allowed us to determine the vegetation aboveground dry biomass for each plant association in g/m^{2}.

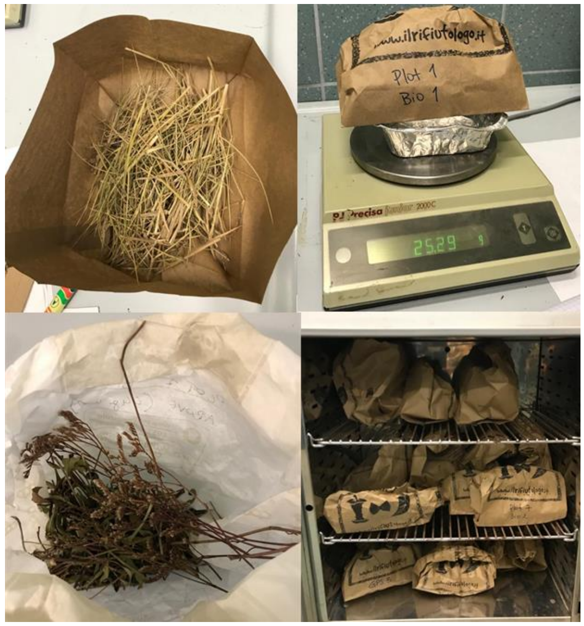

Figure 13 Vegetation samples placed in paper bags for drying in the laboratory

2.4.2 Soil for bulk density analysis

Because the soil samples were frozen, they were first removed from the plastic bags and placed in aluminum trays. Each aluminum tray was identified and weighed while empty. After the samples were placed in the tray, they were placed in the oven at a temperature of 105° C for 72 hours. The weight of all samples was checked twice daily to determine when they were stable.

Once the weight of each sample stabilized, they were removed from the oven and weighed. After the weight of the sample with the aluminum tray was recorded, the samples were placed in plastic bags, divided into smaller pieces, and identified as we can see on Figure 14, preparing them for the Soil organic carbon though from Loss of Ignition (LOI) analysis. The density was calculated dividing the mass of the dry sample Ms (g) by the volume V (cm3) of the original sample obtaining the results in g/cm3 shown in the table in appendix 6.5.

$$BD = Ms / V$$

`

Figure 14 Samples on the field then dried and broken into smaller pieces for further processing

Bulk density was calculated for a total of 27 of the 30 samples collected. Some replicates did not reach the laboratory, so we assume that they were mixed with samples from other projects at the time of storage in the freezers or were lost for some reason. The weights were checked regularly.

2.4.3 Soil organic carbon though for loss of ignition (LOI) analysis

Once the soil samples were fractionated into small pieces, we prepared them for loss on ignition (LOI) analysis of soil organic carbon. The first step for this analysis was to run all samples through a laboratory grinder to homogeneously reduce the size of the stones to 2 mm, see Figure 15**.**

`

Figure 15 Laboratory grinder, 2 mm soil sample and samples in a part of the LOI procedure

After processing, they were kept in plastic bags properly labeled with plot and bio. This analysis is complex; it requires a lot of attention throughout the process and also cannot be done alone, so it was always necessary to have at least two people working on it for proper execution. The sample preparation takes about 5 hours, the combustion of the organic matter in the furnace takes exactly 8 hours and then another 8 hours of waiting until the temperature of the oven has dropped so that the samples can be handled again. A table is presented in appendix 6.3 showing the analysis procedure step by step, the corresponding observations to be taken into account at each step, and the timing we used to optimize the work. This work was carried out by 4 people, so this list was created by the team to always have it as a memory aid, to schematize the analysis and thus perform it in an organized manner on all samples. The formula for calculation of LOI used was:

$$\%LOI = 100 - \%ash$$

Soil organic carbon was calculated on a total of 27 samples. The same samples used for the bulk density calculation were then used in this step and because they were not found in the previous step, consequently this calculation could not be achieved. In the calculations performed on 26 samples, we obtained a consistent result. In the sample located on plot 4 bio 1, the result obtained was very different from that of the other two replicates bio 2 and bio 3 carried out in the same area, which is why this result was not considered in the present work. All the results are detailed in the table in appendix 6.6.

2.4.4 Belowground for dry biomass analysis (g/m^2)

Working with the soil samples for the belowground biomass study consisted of thawing the samples by letting them stand in hot water for about 15 minutes, paying close attention that the plastic bags did not leak to avoid the risk of losing plant tissues. The second step was to remove all the soil contained in the sample. For this purpose, two sieves were used, the first with a of 1 mm stainless steel woven and the second with 500 µm that served as a barrier to all kinds of vegetable matter present in the samples as shown in Figure 16. Run the water through the sieves until no traces of soil remain and only organic matter is observed. After all the soil had been removed, the organic matter was placed in aluminum trays and we used the same procedure as for dissecting the aboveground vegetation. The difference between the quantity of vegetation remained after removing all the soil on the “first”, “second” and “third” part can be seen in the Figure 17. The trays were placed in the oven at 70° C for 72 hours until the weight was stable. The trays were weighed with vegetation and then without vegetation to obtain the net weight of vegetation by subtracting the weight of the trays. All the samples reached weight stability within 72 hours.

Figure 16 Belowground samples after removing all the soil

A total of 58 samples were analyzed the results are shown in appendix 6.7. The samples taken in plots 1, 2, 3 and 4 contained only one part, which was called "first part" and corresponded to centimeters 0 - 10 of depth. In the case of plots 5, 6, 7, 8, 9 and 10, where sampling was done with a deeper core, the results are presented in three parts, designated as "first part" at a depth of 0-10 cm, "second part" at a depth of 10-20 cm and "third part" at a depth of 20-30 cm. The BGB values were calculated first in g/m2, each result representing a value of 10 cm in depth, since this is the value represented by each sample collected. In order to represent them in a better way and

`

thus obtain unanimity in the data, given that in the first plots only the first part is available, once the data were grouped by plant associations (see results), an estimation of the second and third part was made in the plots where this data was missing, using data available in other plots. This made it possible to obtain BGB g/m2 in 30 cm depth in the totality of the samples to perform the analyses presented in the results.

Figure 17 Vegetation samples for the calculation of BGB visual comparison between the 1^{st}, 2^{nd} and 3^{rd} parts

2.5 Ground truthing data

2.5.1 GNNS Points

During data collection, a total of 563 points were collected using GNNS technology to ensure accuracy. These points were located in the center and corners of the plots, in the middle of each target to be used as ground control points, and as points to locate plant associations distributed throughout the salt marsh. These data were used as a reference source for analysis, both for their accuracy and for the observations made during the survey, i.e., they not only contain very accurate x, y, and z information, but also represent the reality we observed at the time of the survey. The spatial reference used in these points is Transverse Mercator projection, datum WGS 1984 UTM Zone 33N with geodetic vertical units in meters.

2.5.2 Othophotos and Digital Surface Model (DSM) - Structure from Motion technique

Two products of utmost importance for this work are the orthophotos and the digital surface model (DSM) extracted from them. Both were created by Archetipo and delivered as final products already processed with the use of Agisoft Metashape software, a stand-alone software product that performs photogrammetric processing of

`

digital images and generates 3D spatial data. The orthophotos were taken with a an L1 camera with a 20 Mpx sensor onboard of a DJI Matrice 300 RTK drone) at a flight altitude (above ground level) of 100 m, a speed of 5 m/s, a lateral overlap of 80%, a frontal overlap of 80%. The automatic acquisition mode image alignment was done by point cloud optimization through ground control points insertion so that a detail orthomosaic was created. The projection of the topographic survey was done in the UTM planar system and the calculation of orthometric elevation in meters (a.s.l.) using IGM (Military Geographic Institute) grid with planimetric accuracy +/- 2 cm and elevation accuracy +/- 4 cm with respect to the I-order leveling network. The properties of the orthophotos provided are as follows: 3 bands with cell size in x and y of 0.02 m, the file with a size of 3.17 GB in TIFF format, the projected coordinate system WGS 1984 UTM Zone 33N and the linear unit in meters. The resulting product can be seen in Figure 18.

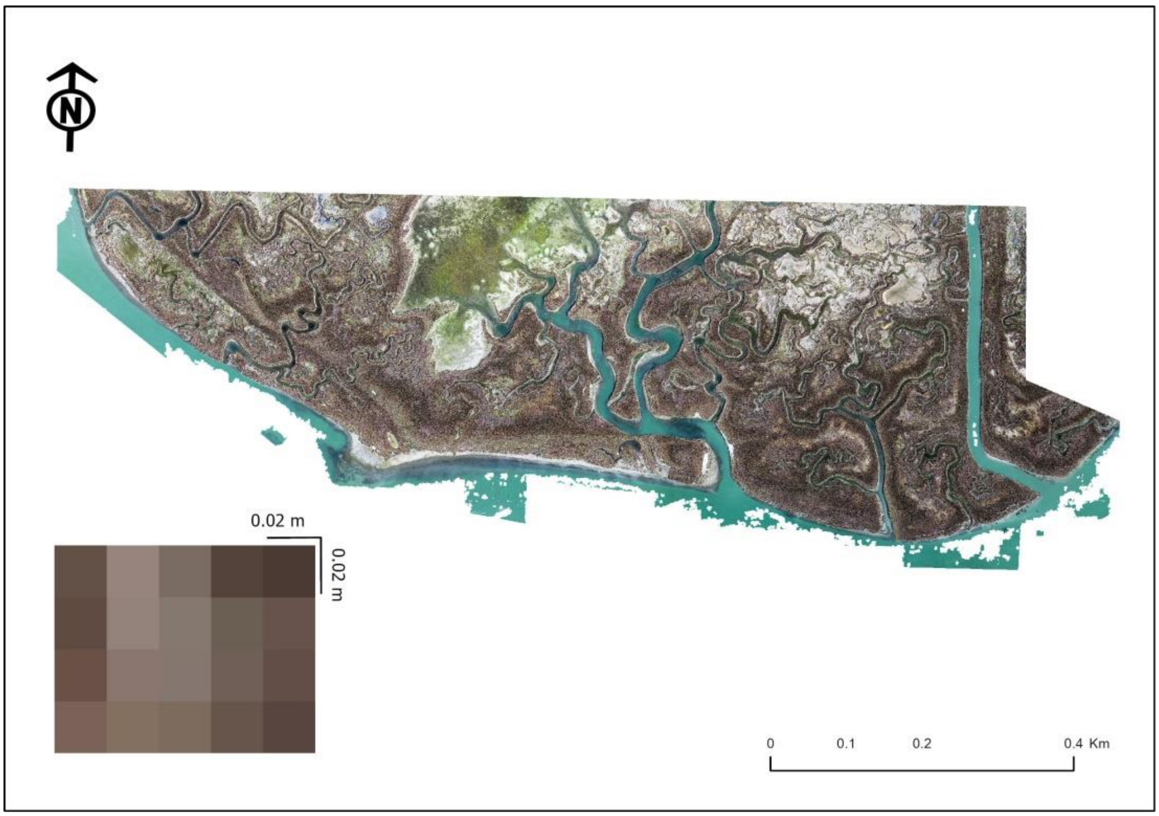

Figure 18 Orthomosaic provided by Archetipo

In order to ensure the accuracy of the digital surface model, 28 ground control points distributed throughout the surveyed area were used. The properties of the DSM are as follows: 1 band with cell size in x and y of 0.04 m, the file with a size of 1.06 GB in TIFF

`

format, the projected coordinate system WGS 1984 UTM Zone 33N and the linear unit in meters, the resulting product can be seen in Figure 19.

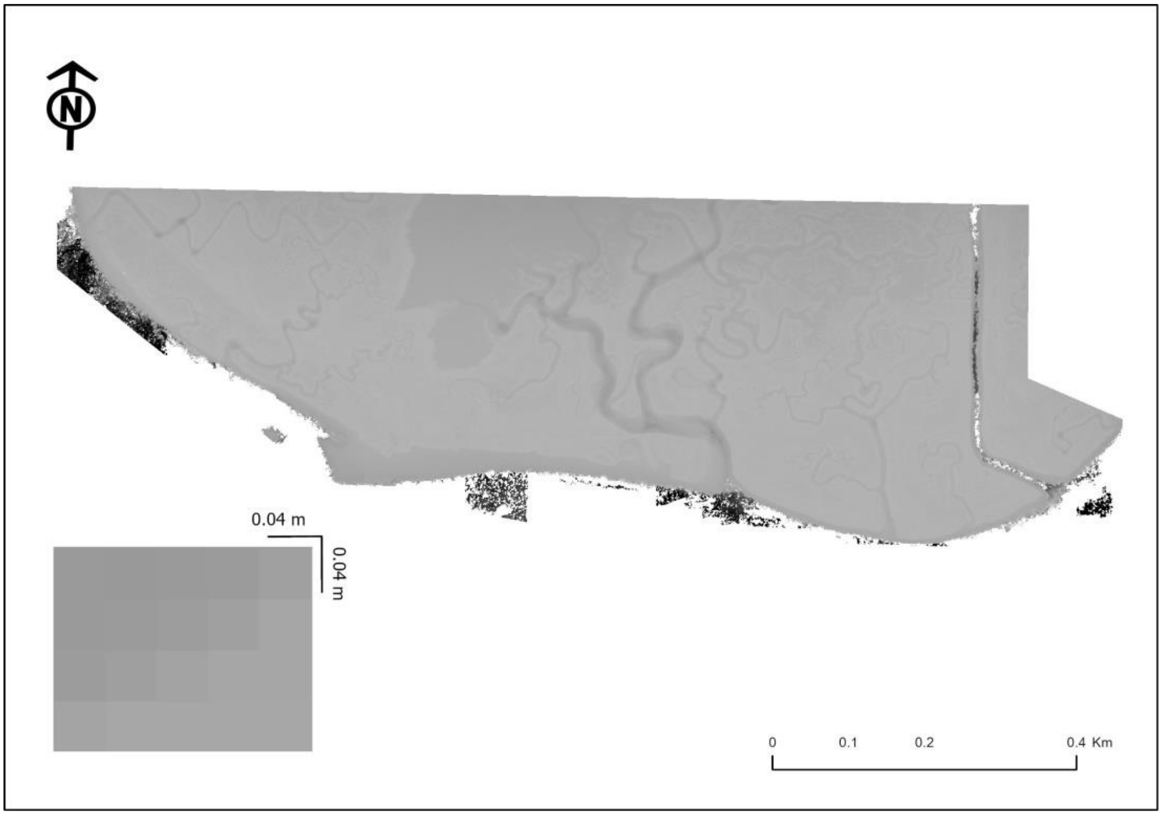

Figure 19 Digital surface model provided by Archetipo

The orthophoto served as the visual basis for the entire work, as a guide and for locating and observing the entire study area, as it has excellent spatial resolution. The DSM served as a source of accurate information about the surface on which we worked and was essential for comparison with the LiDAR cloud, since both have very accurate Z values. For this purpose, the extraction of Z from each pixel was performed by 77centroid points to which the Z value was assigned, as shown in Figure 20; Z-extractions were performed in the reference zones, in this case in 20 targets used to generate ground control points. These targets have a size of 50 cm x 50 cm and we know that they represent an area without vegetation, i.e., it is assumed that the Z values at these locations represent the soil.

`

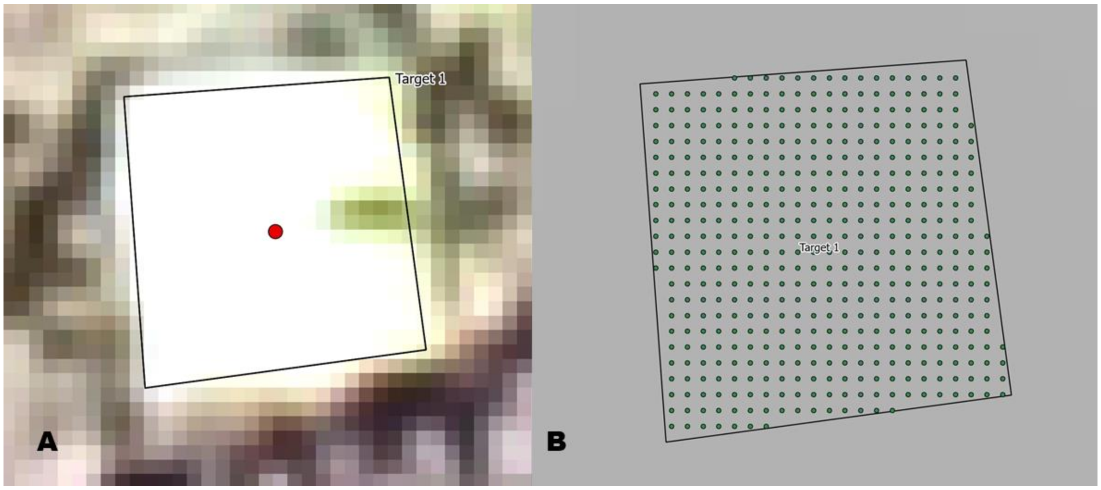

Figure 20 Location of target 1 using an orthophoto, area design of 50x50 cm used for ground truth analysis, site of the ground control point on the target (a) Extraction of Z from each pixel of the DSM, in this case target 1 as an example (b).

2.6 Lidar data acquisition

LiDAR data were acquired by Archetipo with flight parameters of acquisition at a flight altitude (above ground) of 100 m, a speed of 5 m/s, a lateral overlap of 30%, non-repeating scan mode, 180 Hz frequency, 3 echoes, and then pre-processed by them before providing us with the final product for analysis. LiDAR survey alignment and scan optimization was performed using DJI Terra - Pro software. Overlap elimination was performed using Terrascan software: this software uses the overlap points to optimize the scans by averaging the positions between the points of one scan and the next scan with opposite direction. Georeferencing was done with Terra Match software by inserting ground control points (the software calculates the difference between the heights of the laser and the measured points (ground control points) and applies a displacement without deforming the cloud.

Two products were supplied by Archetipo, first a cloud with 63,642,857 points, an average distance between points of 0.096 m and a weight of 2,063.62 MB that during the analysis we found that many filters and processing were done before the delivery, so we proceeded with the request of a raw cloud and with less filters, after which we received a second product with 82,550,455 points, an average distance between points

`

of 0.074 m and a weight of 2,676.69 MB. The second product was used for all calculations performed in this work, the details of which are given in Table 3.

Version format	1.2 /3
Point count	82.550.455
XY Coordinate System	WGS_1984_UTM_Zone_33N
Z Coordinate System	No projection
Has RGB	Yes
Has GPS Time	Yes (Standard Time)
Generating Software	TerraScan
Scan Angle	from -35 to 35
Variable Length Record Count	3
Classification Codes	
1 Unassigned	78.077.142 points
2 Ground	4.473.313 points
Extent	
X Minimum	300534.245
X Maximum	301830.518
Y Minimum	5038918.037
Y Maximum	5039461.729
Z Minimum	-0.771
Z Maximum	13.891
Returns	
1^{st}	82.537.320
2^{nd}	845
Last	82538093
Single	82537248
First of Many	72
Last of Many	845

Table 3 Characteristics of the LiDAR data used for the analysis of the present research

2.6.1 LiDAR data processing

A student license of ArcGIS Pro 10.8.2, geospatial software for viewing, editing, managing, and analyzing geographic data, was used to analyze and evaluate the LiDAR product. This software has a complete set of tools for managing LiDAR data. At the beginning, it was necessary to explore all the functionalities and possibilities of the software in order to find the most suitable method for the objective of the investigation

`

which is to collect from the cloud of points the data for the application of the formula for the estimation of the Leaf Area Index (LAI) precisely in the area of the 10 plots from which samples were taken in the field and analyzed in the laboratory. LAI is calculated using the formula below, this formula is based on the calculation of the probability of penetration of the laser beam through the vegetation to reach the marsh ground where R_g represents the number of points that reached the ground (groundpoints) and R_t total number of points within a specified area (Richardson *et al.,* 2009; Houldcroft *et al.,* 2005). The formula is defined as follows;

$$LAI = -\cos(\theta)\ln\left(R_g/R_t\right)/k$$

where θ corresponds to the zenith angle (scan angle of the sensor) and k represents the extinction coefficient $(= 0.5)$ (Campbell, 319 1986; Houl *et al.,* 2005). Considering most of the available literature (Campbell, 1986; Yousefi Lalimi *et al*., 2017), we assume that all the scan angles are equal to zero θ=0. To apply this formula, we will then try to identify how many points reached the ground (Rg) and how many did not reach the ground (Rt) in the LiDAR cloud using all the data collected (*in situ* and remote sensing) in the same areas where the samples were taken in the field (plots) to make comparisons between them.

What immediately stood out was the software's ability to process a large amount of data without difficulty, as there were no problems navigating through the extensive point cloud. It was also very noticeable how easy it was to perform quickly analyzes to observe the data we had throughout the study area. In Figure 21 we can see the results of mapping the data. With just a few steps, ArcGIS allows me to quickly view the LiDAR cloud with various inputs. For the present work, an attempt was made to use the tools of the ArcGIS Pro software in order to fully exploit them and to develop a methodology based entirely on this software. Methodological tests were also carried out with the tool Rapidlasso LASTools, which is available as a toolbox for ArcGIS Pro, in order to make comparisons and to be sure that the processes used in ArcGIS were producing correct results.

`

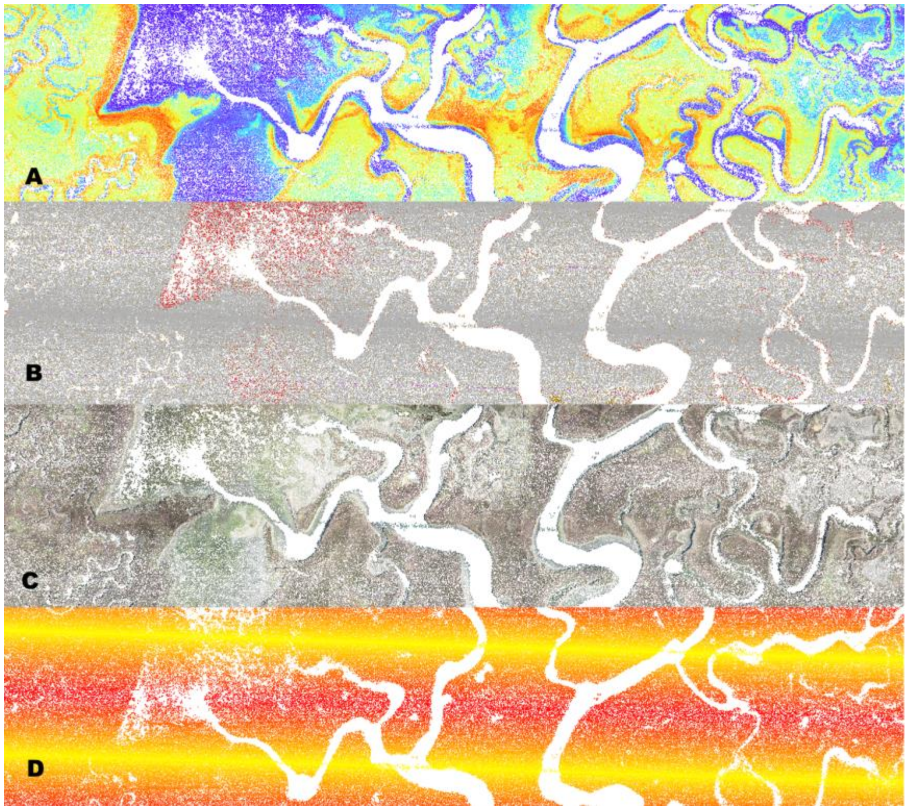

Figure 21 Visualization using elevation as input (a) visualization using classification as input (b) visualization using RGB as input (c) visualization using scan angle as input (d)

The first analysis done in the point cloud was to reclassify the points, since originally we only had two types of classifications: unclassified and ground. To make sure there were no overlaps in the cloud and to filter them out, we used the “Classify LAS overlap” tool. Then to reduce the noise we used the tool “Classify LAS Noise” and as a result we got two new classifications. To improve the classification of the ground points and keeping the points already classified as ground, the “Classify LAS ground” tool was used to obtain the most accurate classification within the capabilities of the software. The process used can be seen in Figure 22.

`

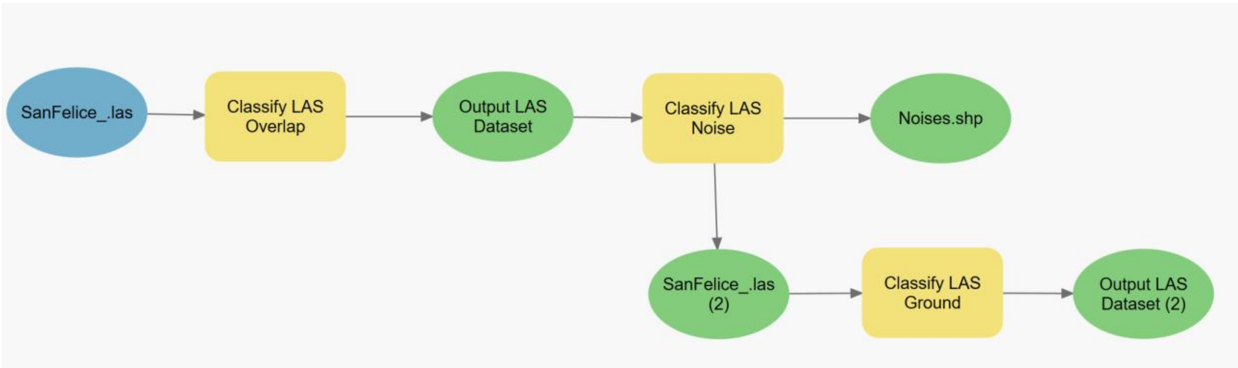

Figure 22 Modelbuilder of the first processes performed on the LiDAR point cloud

The next necessary classification at this point was to locate and remove Outliers, for that purpose ArcGIS Pro has a tool called Locate Outliers. However, the results were not reliable because a very large number of points in the cloud were identified as outliers and for some reason almost all points within our area of interest were eliminated. Consequently, the path chosen in order to continue with the analysis was to export all LiDAR points of the areas of interest and proceed with the analysis in Excel spreadsheets. The export, of data from all areas of interest, has been performed using the procedure shown below in Figure 23 using ArcGIS Pro, and to compare and check if the data was exported correctly, the tool Rapidlasso LASTools Las2txt was also used on the same data. For data export, the simplest way was to use the Las2txt tool, but as mentioned above, one of the objectives of this work was to develop a methodology using only ArcGIS Pro tools.

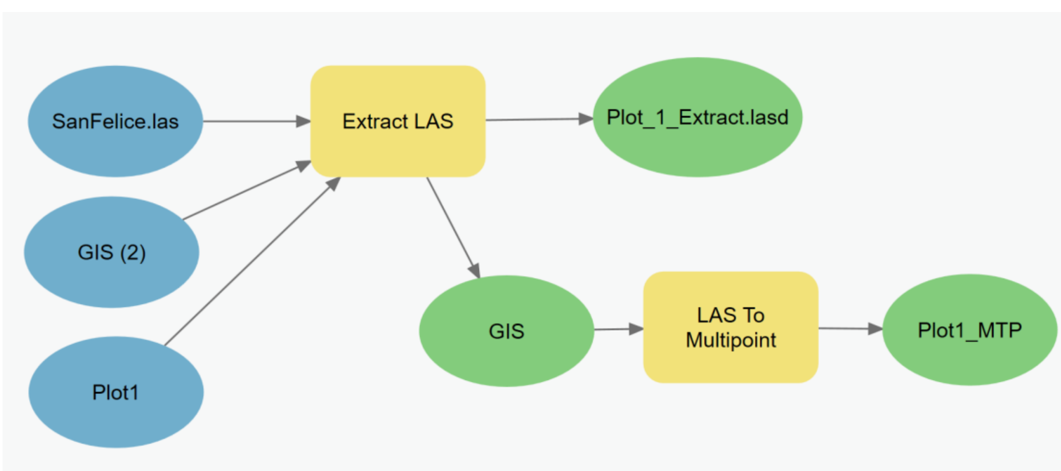

`

Figure 23 Modelbuilder of the extraction of points from an area of interest, plot 1 in this case, and transformation of the LiDAR points to a multipoints file

When transforming the LiDAR data to a Multipoint file, it was noticed that the data associated to the LiDAR points that were necessary for my analysis were not found in a manageable way in the attribute table. This is because they were stored in cells with BLOB format. For that reason, the next step was to edit the exported Multipoint file and through the Explode tool, separate the multipart feature into individual features in order to assign values to each particular point, our interest was to obtain XY and Z for each point. Once each point was already individually represented in the attribute table, it was preceded to the attribution of XY and Z, the complete process is shown in Figure 24.

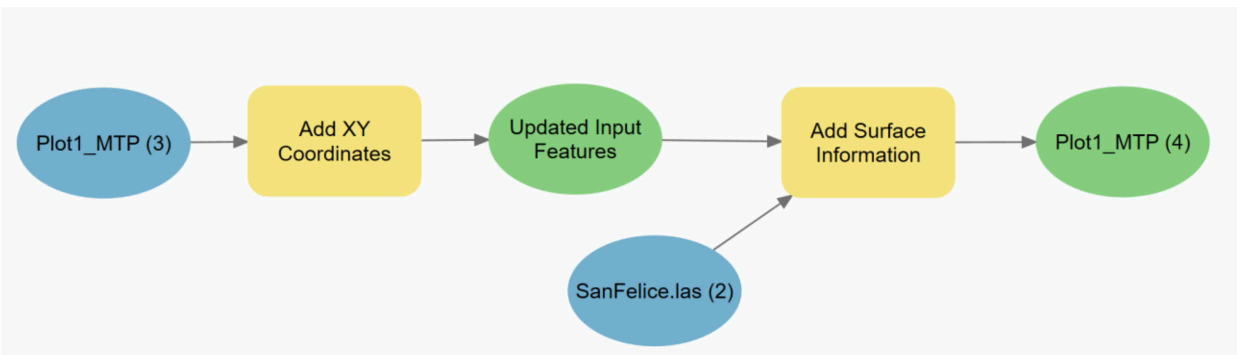

Figure 24 Modelbuilder of the processes used for the assignment of XY and Z values to each point, plot 1 as an example

At this point the data were already in the attribute table, and from the file in .dbf format associated to the shapefile it has been possible to export all the values related to each point and thus perform a deep and detailed analysis of each area using Excel spreadsheets. A more in-depth and less automated analysis of identification of outliers was performed using quantiles analysis to filter them out and to continue with next steps of the analysis, always with the objective of identifying ground points as accurately as possible. This analysis consisted of identifying the point at the 20th percentile as well as at the 75th percentile in order to calculate the Range IQR, i.e., the range between the upper quartile and the lower quartile, marked in green in Figure 25. Then the upper and lower whiskers were determined. At this point, the quartile groups were divided into "group 1," "group 2," "group 3," and "group 4," as shown in Figure 25. The points that were in quantile groups 1 and 4 were considered as outliers.

`

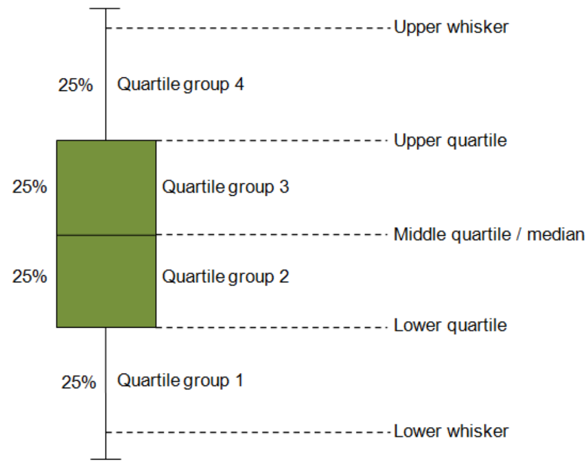

Figure 25 Graphical description of the quartile group division used to identify outliers.

3 RESULTS AND DISCUSSION

3.1 Field campaign and laboratory

Since the final goal of the present work is to calculate LAI using LiDAR and then compare it with the results obtained using AGB in the laboratory, special attention was paid to these calculated data for further analysis. Many types of analyzes and demonstrations can be performed with the obtained results, as they are very numerous. However, since the interest of the present work is focused on the Z-heights of the vegetation above the ground, analyzes carried out concentrate only on this part of the data.

Previous studies in the same study area describe the profile of salt marshes as shown in Figure 26. From the highest parts near the channel, the height decreases in the inner parts (Silvestri *et al.,* 2005). The distribution of species is also not random, but spatially coherent and organized in patches, as mentioned by (Chapman, 1976; Silvestri *et al.,* 2000; Marani *et al.,* 2003, Silvestri *et al.,* 2005) and as also shown in Figure 26.

`

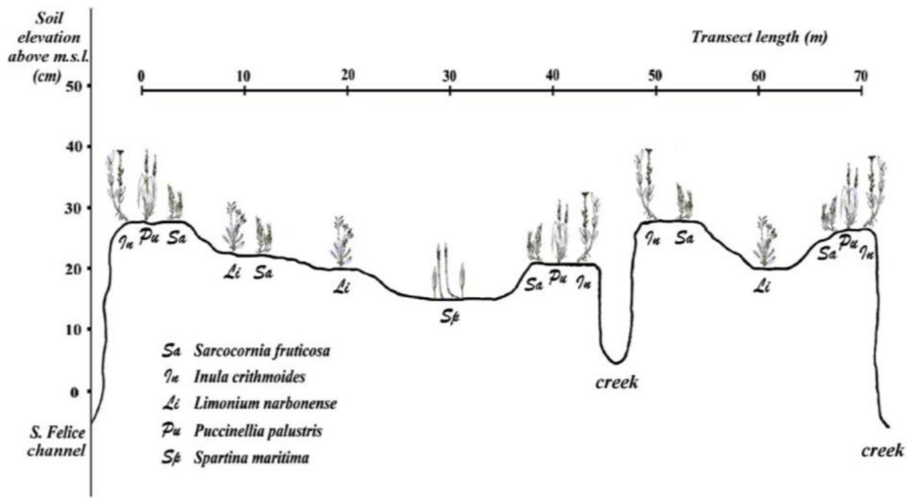

Figure 26 Soil profile and distribution of vegetation species according to height in cm above m.s.l. (Source: Silvestri *et al.,* 2005)

For the analysis of the collected data, they were grouped according to their frequency, observed in the field. The groups used corresponds to the mail vegetation associations typical of this area, and are described as follows Sarcocornia > = 80%, Limonietum (Limonium > = 80%), Spartina maritima > = 50% and < 70%, Inula > = 50%, Spartina anglica > = 90% and Salicornia veneta > 40% with soil.

As a result of the distribution of the association of species in relation to the soil elevation, shown in Figure 27, a perfect concordance was found with what was mentioned by Silvestri *et al.,* 2005, that the associated elevation values has a strong dependence of vegetation presence on soil elevation. The vegetation sequence of species with increasing soil elevation are: Spartina (abbreviated *Sp. Mar* in the figure) grows on the lowest soils, Limonium (abbreviated *Lim. nar* in the figure) over, slightly higher areas, Sarcocornia (abbreviated Sar. *fr in* the figure) on even higher soils. The highest AGB values are found for *In. crit.* and *Sar. fr*., while the lowest value is found for *Sal. ven.*

`

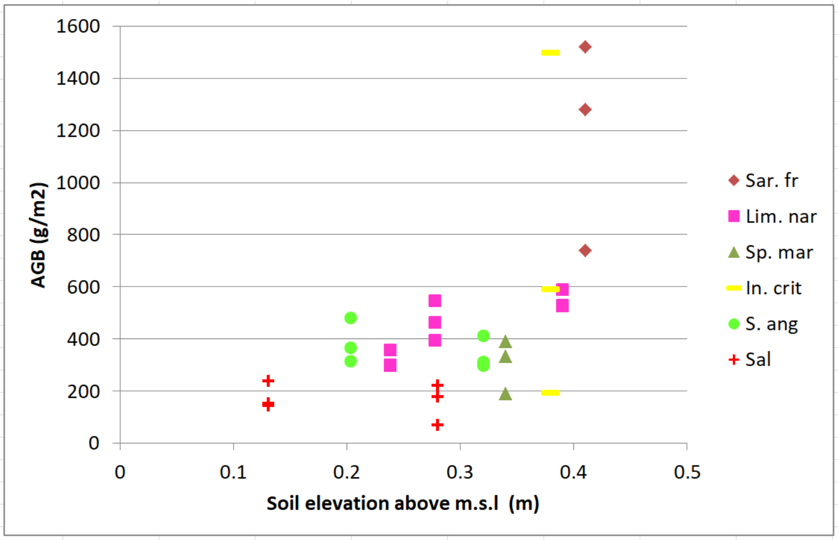

Figure 27 Relationship between aboveground biomass (g/m^2) and soil elevation above m.s.l (m)

Considering the calculation of BGB, the Limonium association has considerably higher values in relation to the others, it is located in the middle zone of the marsh. Taking into account that a depth of 30 cm in depth has been considered, in this graph it can be observed that the Limonium association is the one that accumulates the highest amount of organic matter, and this occurs more or less between 0.25 and 0.40 m above sea level, and this can be confirmed with the graph in Figure 28, where we can see that the highest amount of LOI is found in areas where this plant association is abundant.

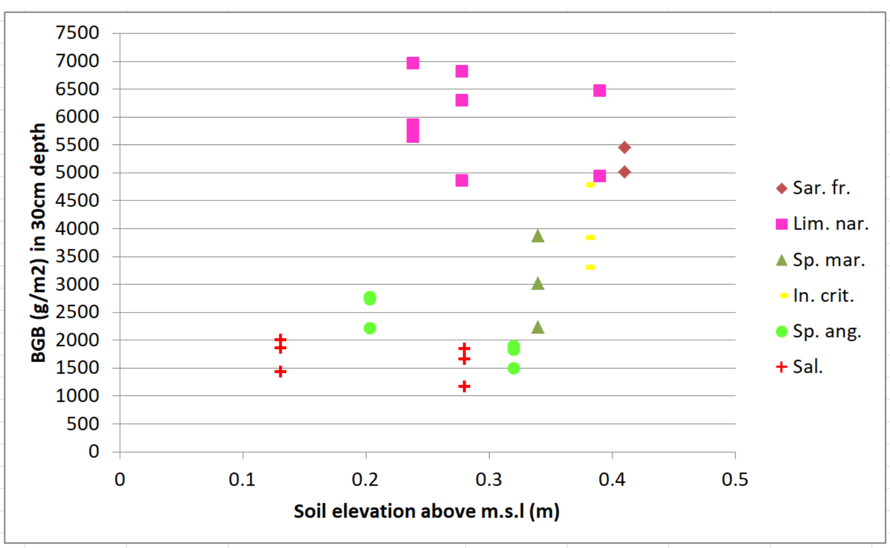

Figure 28 Relationship between belowground biomass (g/m^2) and soil elevation above m.s.l (m)

`

This confirms the large contribution of Limonium to the organic matter that accumulates in the soil. Limonium is a protected species, and its value for the Venice marshes is very high also for its carbon sequestration effect.

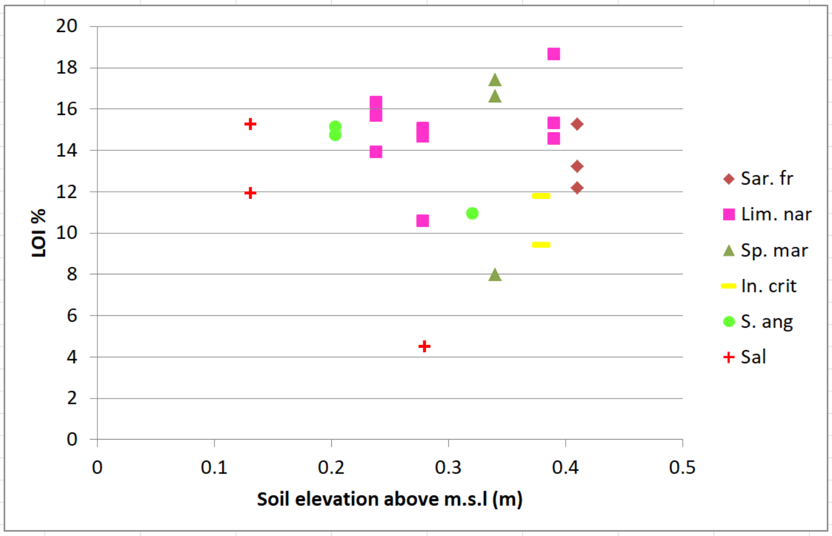

Figure 29 Relationship between LOI and soil elevation above m.s.l (m)

The graph in Figure 30 shows the relationship between AGB and BGB in the three parts studied: first part, 0-10 cm depth; second part, 10-20 cm depth; and third part, 20-30 cm depth. From this diagram, it is evident that the greatest amount of BGB is found in the first 10 cm of thickness. This confirmation makes the decision made during the field survey to change the core and go deeper into the soil worthwhile; if we continued with the core used during the first days, this would not be detectable. However, the relationship between AGB and BGB that exists in the plant association known as "Limonietum", which in this case represents samples with more than 80% of Limonium species, is noteworthy. In this case it can be seen that maintains very high values in the second part of the BGM. It can be concluded that in places where this species occurs, there is a much higher amount of carbon stock in the soil than in other places. As mentioned above, we can say that Limonium occurs at medium heights as a function of soil elevation, not at the lowest and not at the highest parts of the marsh.

`

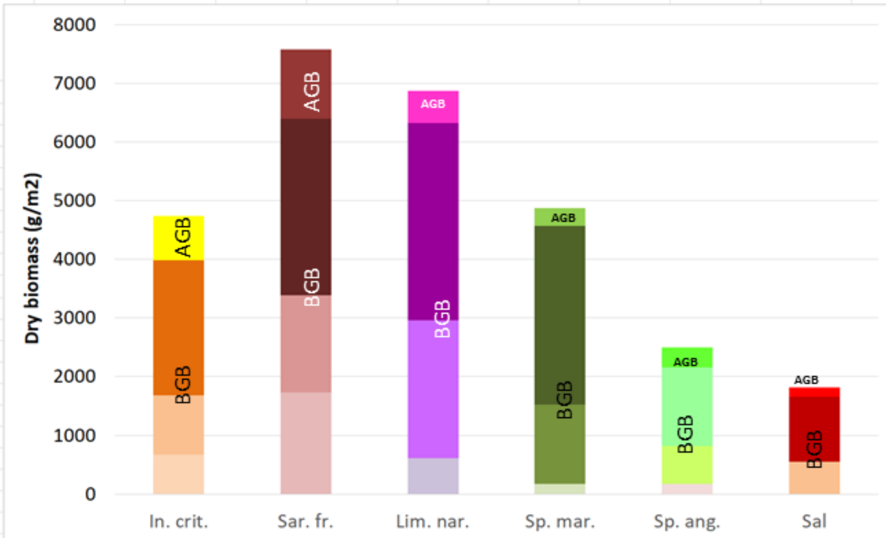

Figure 30 Comparison between AGB and BGB in its various parts, for each plant association studied in this work

The results obtained in relation to bulk density shown in Figure 31 confirm that the highest values are found in the highest areas of the marsh, even though the relation is weak. The differences between the different plant associations are not very great, but there is a clear increase in the values of the species in the higher zones and a decrease in the species in the lower zones of the salt marsh. To conclude, the results show that the highest BD value was observed in the association where the Inula species predominate and the lowest in the association where the Salicornia species predominate, being those found in the highest and lowest zones of the salt marsh in terms of height.

`

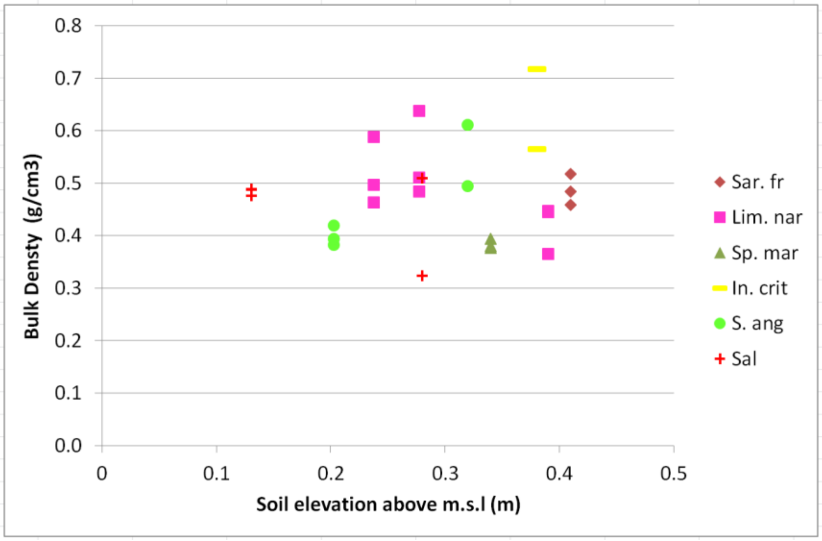

Figure 31 Relationship between bulk density (g/cm^3) and soil elevation above m.s.l (m)

3.2 Comparison of data extraction methodology using ArcGIS and LAS2txt tool

In order to confirm the effectiveness of the methodology developed in ArcGIS for the LiDAR cloud data extraction, a comparison was made between the data extracted with the Las2txt tool and the data extracted with this software. Data export tests with both methodologies were performed within the 1x1 m polygons corresponding to the plots. All points within this area were extracted with both tools and then compared. For this purpose, an Excel spreadsheet was created comparing the XY and Z values extracted. The efficiency of using ArcGIS to extract data from a .las file was confirmed, as the data extracted with both tools matched completely in all cases. The only disadvantage of the method in ArcGIS is that it involves many steps, requires a lot of attention in each of them and the correct configuration of parameters. The Rapidlasso LASTools tool, however, enables a very user-friendly export of the data records to a .txt file in a direct way. A comparative example of data exported using both tools are shown in appendix 6.9.

3.3 LiDAR cloud quality analysis from bare soil zones

To analyze the quality of the LiDAR cloud, a series of Z-analyzes were performed at six points on the cloud at locations without vegetation. The orthophoto was used to locate the points, from where the data were exported and then organized in Excel. The following calculations were performed: maximum Z containing the outliers, minimum Z containing the outliers, and from this the cloud thickness with outliers was calculated.

`

Then the outliers were filtered out and the maximum Z, minimum Z, and cloud thickness without outliers were calculated.

The six points were selected for the present analysis at locations for which a known Z value was available from a GNSS field measurement. Using the Z data from the known point, comparisons were also made in terms of the mean Z value of all points in the area, assuming that since it was a vegetation zone, all points in the cloud should have represented the ground. For an example, a portion of the data in the area labeled "Bare Soil 1," which is 1x1 m and contains 195 points, can be seen in appendix 6.10, as well as the calculations made with it. All calculations with their repetitions cannot be presented in this work since the spreadsheets are very extensive since every analyzed area contains between 190 and 325 points, so they cannot be included in the appendix of this document. In case of interest they be sent or uploaded to a cloud.

After performing the calculations on the six points, it was noticed that the results of the cloud thickness, even after removing the outliers, were very high in all cases as it can be seen in Figure 32. With the accuracy expected from a LiDAR cloud, it is very remarkable that in an area where there is no vegetation or any element representing a height in Z, a variability greater than 0.1 m is obtained. Another factor that stands out in this case is the large difference between the variabiility with and without outliers, which gives us an indication of a very high level of noise. For all of these reasons it was decided to perform a further analysis of the quality of the LiDAR cloud. The results of the calculations can be found in the appendix 6.8.

`

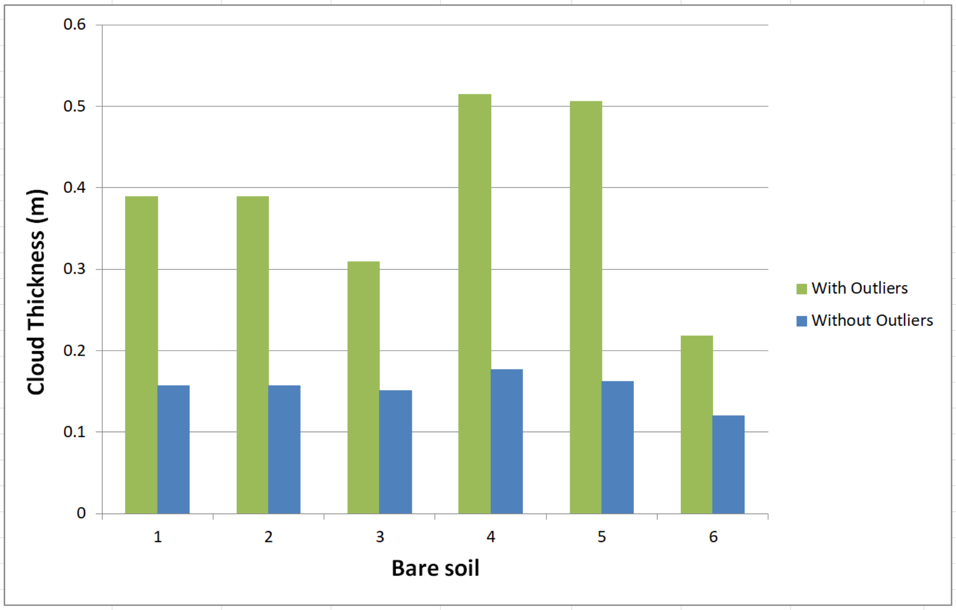

Figure 32 Cloud thickness with outliers and without outliers in the 6 bare soil zones analyzed

3.4 LiDAR cloud quality analysis from GCP targets

For the 20 CGP targets (location shown in Figure 6 of this document), the same calculations were performed to control the quality of the LiDAR cloud. First, outliers were identified in an Excel spreadsheet, and then the maximum and minimum Z with outliers, the maximum and minimum Z without outliers, and the calculation of the cloud thickness in both cases were calculated.

In this case, the control area, sequentially labeled "control 1 to control 20", was 0.5x.05 m and contained between 30 and 75 LiDAR points inside. These control areas (targets) were in known locations because they were positioned by us in the field, which provided assurance that there was no vegetation on them. Using them a better representation of the entire extent of the LiDAR cloud was obtained because the so-called controls were distributed over the entire study area.

Again, the results showed that the cloud thickness even without outliers had high values, as presented in Figure 33. Here we could see that, for example, in controls 10 and 11 the thickness of the cloud is more than 0.20 m, but in control 12 it is less than 0.10 m. This shows inconsistencies, so we can assume a low quality of the LiDAR data.

`

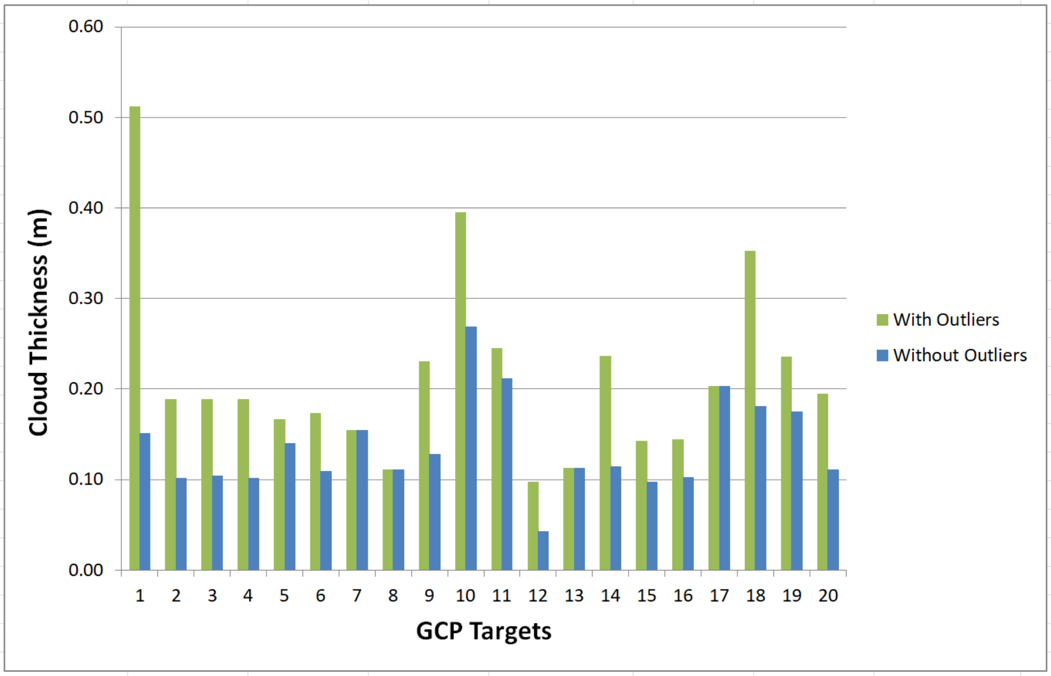

Figure 33 Cloud thickness with outliers and without outliers in the 20 GCP zones analyzed

In order to better understand the Z-behavior of the points where cloud thickness was high, the points were visually analyzed using the ArcGIS 3D visualization tool. As an example can be seen in Figure 34 that the points in the area designated as control 1 actually have a height that does not correspond to reality, i.e., an area without vegetation we can also see that most of the points did not reach the ground, represented here by the gray surface corresponding to the DSM.

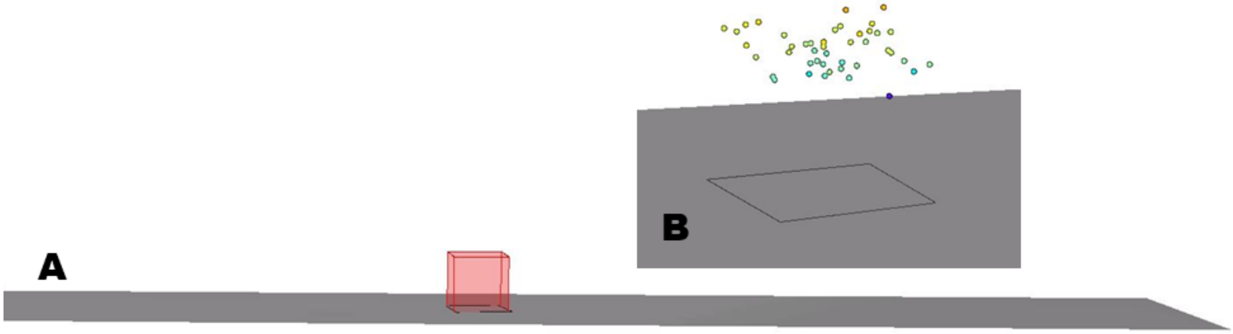

Figure 34 3D view of LiDAR points (b) belonging to the area referred to as Control 1 (a)

Given the results obtained, the extraction of Z from the DSM was performed to make a deeper analysis, taking into account that the DSM reflects the height of the surface. Since it was known that there was no vegetation at these locations, it was assumed that

`

Z from the DSM would represent the ground in this case. To this end, Z was extracted from all pixels contained in each control area. Using this data in the same Excel spreadsheet, the following analyzes were performed: calculation of average Z from DSM, calculation of average Z LiDAR, standard deviation of Z from DSM, standard deviation of Z from LiDAR. A comparison between the Z values of the different sources, LiDAR and DSM, resulted in the Figure 35, which shows the distribution of the Z values of the LiDAR points compared to the Z values of the DSM, these points belong to the area we refer to as control 1, the same one used in the 3D visualization shown in Figure 34.

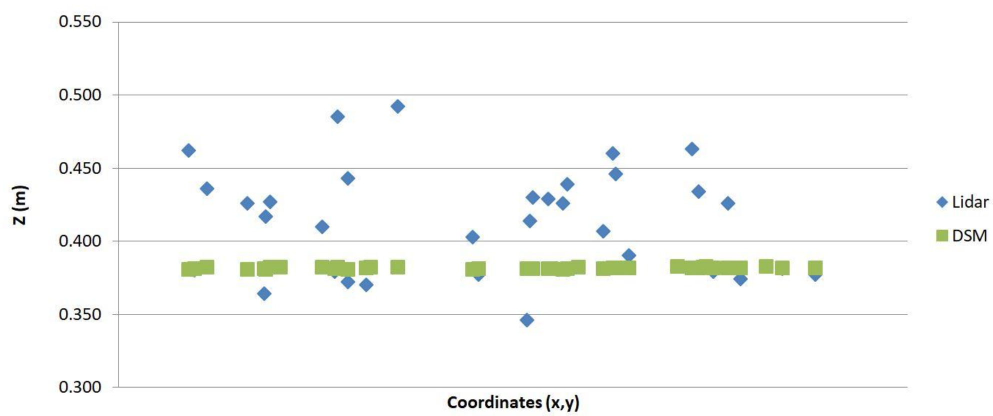

Figure 35 Z-Distribution of LiDAR and DSM data in Control 1

It can clearly be seen that the DSM data represent an area without vegetation, keeping its Z value constant, but the LiDAR cloud does not. It is even possible to observe that there are values that are below the ground. This factor this problem is one of the major drawbacks for this work, because to achieve the calculation of LAI it is important to identify ground and non-ground points, and if this is the representation of an area without vegetation, it would be impossible to identify what each point represents in places where vegetation is present.

In appendix 6.11 an example of how analyzes were organized in the Excel spreadsheet can be found, and a part of input data. Since the calculations are very extensive and there are several repetitions, they cannot be included in this work, but can be requested if necessary. A summary of all the results obtained, referring to all the repetitions performed, can be found in this document in appendix 6.8.

`

Two factors were noteworthy, not only because the results showed that the cloud thickness had high values at sites without vegetation, but also because there was a large difference between the standard deviation of the LiDAR points and the standard deviation of the DSM for the 20 control points. No further quality analyzes were performed, and it was established that it was a non-systematic error, i.e., there was no way to correct or estimate it. This fact was reflected in all the replicates performed. Such errors can be caused by a variety of factors, from a mechanical failure of the sensor to a temporary loss of connection to the GNSS reference station network used to correct the points. At this point, only theories can be put forward, but none of them could be confirmed.

To show more clearly the result of the quality analysis performed with the LiDAR data using GCP, Figure 36 shows a representation of the mean Z height in the LiDAR cloud compared to the mean Z height of the DSM data in the 20 targets used as reference for the analysis. As can be seen, there is no correlation between these data at the individual study sites, but most importantly, it is important to note that the error is not constant so that a possible schematic error, projection error, or other correctable source can be ruled out. Sometimes there is a small difference between the two data; sometimes the difference is very large. For better understanding, the graph in Figure 37 shows the difference between the standard deviation of the two data. It can be seen that the standard deviation of the LiDAR points is almost four times higher than that of the DSM.

`

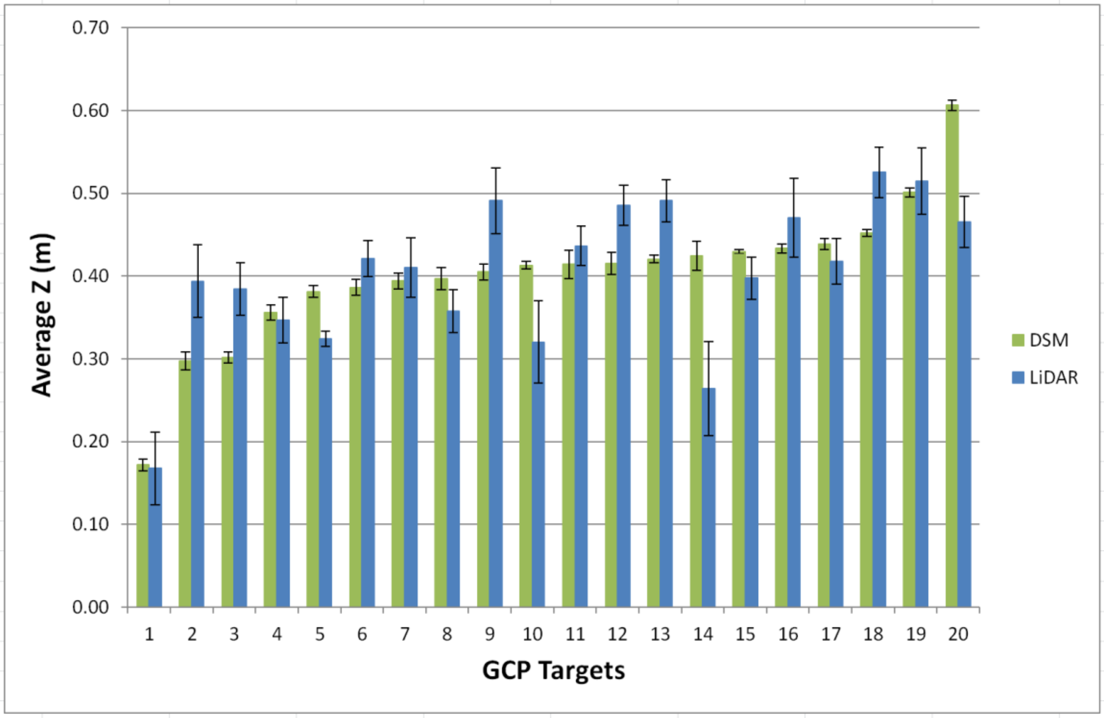

Figure 36 Relationship between average height of LiDAR and DSM data with its standard deviation

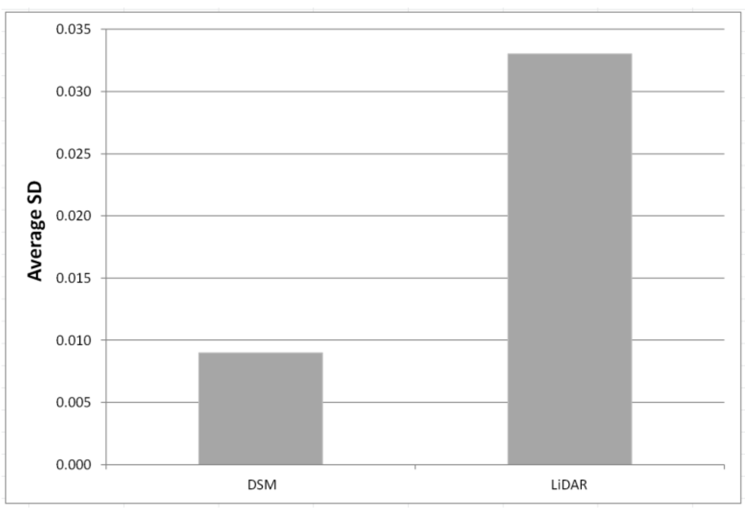

Figure 37 Difference in the average standard deviation between LiDAR and DSM data

`

3.5 LiDAR data analysis on plots

The data analysis of LiDAR in the plots was performed in Excel spreadsheets, as in the two quality analyzes mentioned above: identification of outliers, maximum and minimum Z-value with outliers, maximum and minimum Z-value without outliers, mean of the Z-values of the GNSS points of each plot. In this case, and with the aim of having all the information for the LAI calculation, the mean LiDAR scanning angle was exported, the point-count with outliers and without outliers were also calculated for each plot. For an example of the table used for the calculations, which in this case that belongs to plot 1 calculation, a part of it can be seen appendix 6.12. The full table is available upon request, but since it contains a large amount of data, it is not included in the appendix of this document.

Considering the situation described above, the problems encountered and the lack of reliability of LiDAR data, it was decided to create a diagram to visualize all the points corresponding to LiDAR data in all the plots in Z. In Figure 38, it can be seen each species association assigned to a color. The black points correspond to GNSS points taken in the field and used as a reference for the location of the ground.

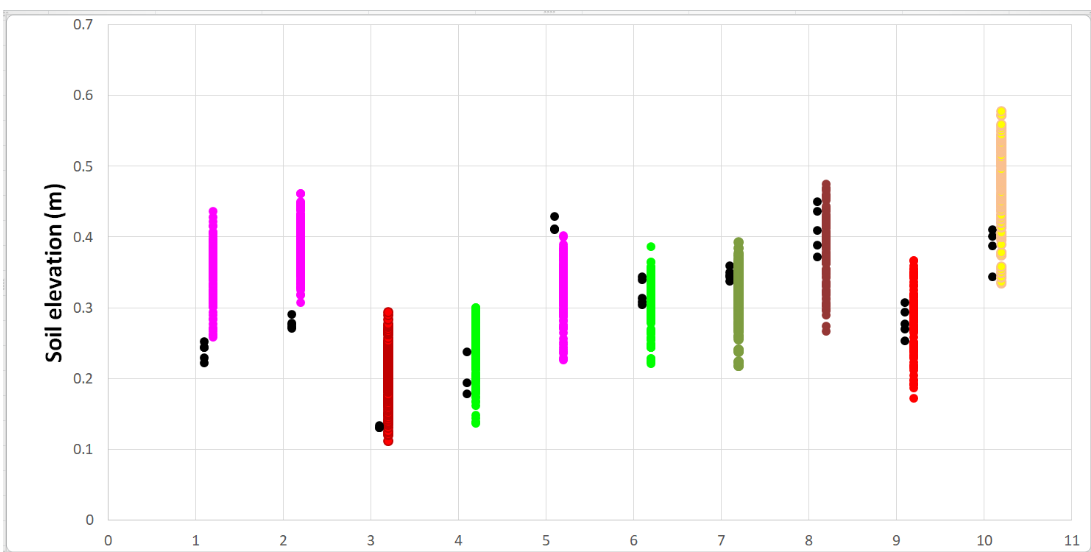

Figure 38 Demonstration of the mismatch between LiDAR data and GNSS points that are used as ground reference.

As we can see, there is not a good match between the data that should be used as ground reference, the GNSS points and the LiDAR points of each plot. Even in some cases, such as plots 5, 6, 7, 8, and 9, most of the LiDAR points are below ground level,

`

which cannot possibly correspond to reality. This confirms that the analysis of the LiDAR cloud, where some discrepancies were found, is also reflected in the plots, which are the data source on the basis of which the calculation of LAI should be performed. It is therefore impossible to rely on calculations performed with such data.

Taking advantage of the reliability of the DSM established in this work, a final analysis, shown in Figure 39, was performed to correlate it to the height of vegetation measured in the field. To determine the actual height, the sum of the Z-values of the GNSS points in each of the 10 plots was added to the height of the vegetation measured in the field. Excellent correlation was found between the two data. This means that the DSM was correctly used as a source of reference data and also opens the possibilities that vegetation characterization can be used with this type of data.

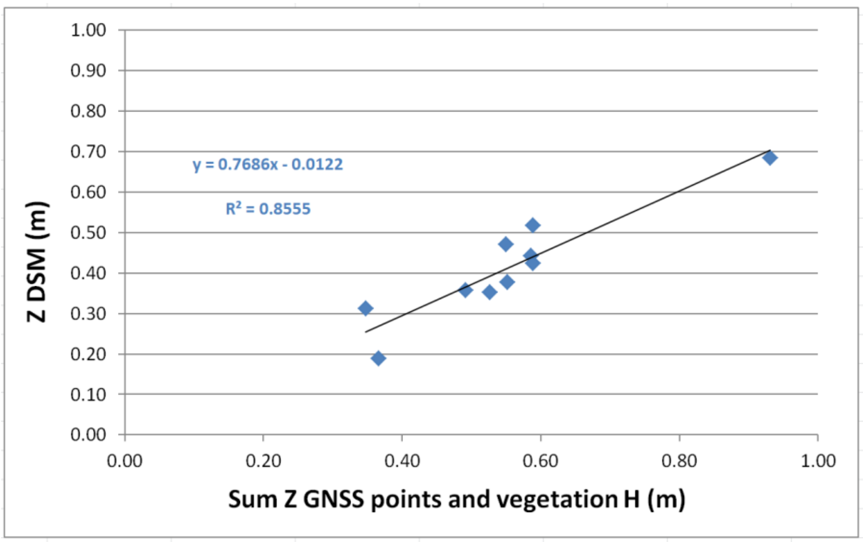

Figure 39 Correlation between DSM height and vegetation height in the 10 plots

`

4 CONCLUSIONS

4.1 Field campaign and laboratory

It is very important that when planning the type of research presented in this work, which involves a large amount of data collection, several aspects must be considered with great attention. In our case, we can say that the results, both organizational and in terms of the amount of data collected, are undoubtedly very good. A small inconvenience was noting the absence of some soil samples at the beginning of the work in the laboratory. At some point in the transport chain of samples to the laboratory, they were lost or mixed with samples from other projects, making it impossible to identify them for analysis. In any case, thanks to the number of replicates for each sample, a good representativeness of the plant associations present in the study area was achieved. It was not possible to analyze the Juncus species because they were not represented in a good percentage on the associations in the samples taken in the plots. It is also important to emphasize that working with many samples and with so many types of analyzes requires a lot of time and at least a good team of collaborators. In this case, two people were responsible for the laboratory analysis of all samples, sometimes with the help of two other people, so that the analysis work was completed in a total of 5 months. But all the work was worth it, because a lot of detailed information about this ecosystem was collected. Worth mentioning is the important information on the BGB. The collection of data from 30 cm depth in this area is something new, although it is a very well researched area; such information with such a high level has never been collected before. Compared to the literature and previous work at this site, good results were obtained.

This work confirms a good agreement with the existing literature, which mentions that the value of the elevations is related to the presence of certain species associations depending on the altitude at which they are found. The succession of species with increasing altitude above m.s.l has been confirmed as follows: *Spartina* occurs mainly in the lower areas of the marsh, *Limonium* in the middle zones and *Inula* in the high zones. The highest AGB value was found for *Inula* in the high zones, and the lowest value for *Salicornia*, which is found in the lower zones. The association *Limonietum*, where considerably high BGB values were observed, confirmed the great contribution of this association to soil organic matter and saltmarsh vertical growth; this species is a protected species in the study area and is protected because of its carbon sequestration effect. The same could be observed in the LOI results obtained in areas where this association is predominant. The BD results showed high values in higher elevation areas of the marsh and lower values in lower elevation areas, although the relationship

`

is weak. The highest BD values were found in areas where *Inula* species predominate, i.e., higher elevation areas, and the lowest values where *Salicornia* species predominate, i.e., the lowest elevation areas of the marsh.

4.2 Working with remote sensing data for characterizing saltmarsh vegetation - LiDAR, DSM and Orthophotos

For the present work, ArcGIS Pro was chosen as the main software for data analysis. This software is robust and powerful enough to work with very large data corresponding to very extensive areas, as was the case in this work. This statement has been confirmed, there is nothing to say against the performance of ArcGIS in this regard. The first obstacle we encountered in its use was exporting the data stored in .las format to a .txt or similar format. The need to export them became apparent when some values did not seem to correspond to reality and a more detailed investigation was required. Another problem arose when it came to making a correct classification of ground points. Since this was a crucial step to achieve the main objective of this work, it was a very big problem. For these cases, the literature consulted recommends the use of a filter called the Progressive Morphological Filter (PMF) to remove non-ground measurements from airborne LiDAR data (Zhang *et. al.,* 2003) that cannot be performed in the software itself. This filter is best suited for vegetation with the characteristics found in our study area. Since this filter could not be performed, the LiDAR data of the points of interest were exported to Excel tables where another type of analysis was performed in order to try to differentiate between ground and non-ground points. This undoubtedly complicated the analysis of the work, because in order to export it, several steps had to be performed, several parameters had to be carefully configured, and since there were several small study areas, the steps had to be repeated several times. From the moment it became necessary to work outside the software, the work became very complicated. It was decided to find the best way to export the data from ArcGIS for use in spreadsheets, since no material was found after consulting forums and searching for information on the subject. This work contributes to the GIS community in this way. The tool used to test the effectiveness of this method, called LAS2txt, is a tool that is not fully open source. It is available to students and researchers, but may not be used commercially, so if for some reason a company or small business working with GIS needs to extract data from a .las using ArcGIS, a precedent has already been set.

Regarding the results found and demonstrated in this work, it is concluded that in order to work with remote sensing data it is crucial to have multiple sources of information for the area under investigation, in our case these were LiDAR, DSM, Othophotos, but also GNSS points taken in the field. Also, it is very important to know the location to be

`

studied as precisely as possible and to take into account the observations made there, in our case we had a lot of data observed and noted in the field. In this study, all the available data were of great importance to confirm the inconsistencies that the LiDAR cloud showed from various points of view and different inputs. The remarkable variation in the thickness of the LiDAR point cloud could be confirmed given the accuracy found in the DSM in both bare ground and GCP areas. The reliable ground points taken with GNSS confirmed the discrepancies within the plots where most of them could be seen below the ground, which would be impossible given the performance of the LiDAR technology itself.

Another important factor to consider is the planning of data collection by drone. It is important to elaborate this work in great detail, with the participation of both the pilots, i.e., the people responsible for the overflight itself, and the professionals who will be responsible for processing and analyzing the data. Excellent communication with the provider of this service will make all the difference in the final product of any analysis performed on the collected data. It is extremely important that a detailed document is prepared after the flight, taking into account all the parameters, both in the field and in the pre-processing of the data before it is delivered to the customer. This document must be complete, as the professional processing the data relies on it to ensure that his results are consistent and, in the event of problems, to better understand the origin of the problem. In the case of this work, problems occurred with the data, the source of which was not known at the time of writing this document. Several hypotheses can be made in this regard, but so far none of them has been confirmed. These problems have meant that the objective of the present work has not been achieved, since the main source of data for it would be the LiDAR data, which, as has been shown in the course of the work, have errors and on which we cannot rely to make a calculation as detailed as that of LAI.

It is recommended that an in-depth analysis of the vegetation characterization of a salt marsh be performed using a DSM created with the SfM technique. The main advantage in this case is the simplicity of the analysis as well as the survey costs.

`

5 REFERENCES

Adam P. (1990) Saltmarsh ecology. In Cambridge University Press, Cambridge UK (pp. 461).

Allen, J. R. (2000). Morphodynamics of Holocene salt marshes: a review sketch from the Atlantic and Southern North Sea coasts of Europe. Quaternary Science Reviews, 19(12), 1155-1231.

Armstrong, W. (1982). Waterlogged soils. Environment and plant ecology, 2, 290-330.

Astronomical tide prediction in Venice (2021) City of Venice Tide Forecast and Reporting Center (pp.16)

Barragán, J. M., & de Andrés, M. (2015). Analysis and trends of the world's coastal cities and agglomerations. Ocean & Coastal Management, 114, 11-20.

Beeftink, W. G. (1977). Coastal salt marshes of western and northern Europe: an ecological and phytosociological approach. Ecosystems of the World.

Belluco, E., Camuffo, M., Ferrari, S., Modenese, L., Silvestri, S., Marani, A., & Marani, M. (2006). Mapping salt-marsh vegetation by multispectral and hyperspectral remote sensing. Remote sensing of environment, 105(1), 54-67.

Campbell, G. S. (1986). Extinction coefficients for radiation in plant canopies calculated using an ellipsoidal inclination angle distribution. Agricultural and forest meteorology, 36(4), 317-321.

Carbonneau, P.E., Dietrich, J.T., 2017. Cost-effective non-metric photogrammetry from consumer-grade sUAS: implications for direct georeferencing of structure from motion photogrammetry. Earth Surf. Process. Landf. 42 (3),
473–486

Chapman V. J., (1964) Coastal vegetation Oxford: Pergamon Press. New York: the Macmillan Company (pp. 83-129)

`

Chapman, V. J. (1975). The salinity problem in general, its importance, and distribution with special reference to natural halophytes. In Plants in saline environments (pp. 7-24). Springer, Berlin, Heidelberg.

Cherry, J. A., McKee, K. L., & Grace, J. B. (2009). Elevated CO2 enhances biological contributions to elevation change in coastal wetlands by offsetting stressors associated with sea-level rise. Journal of Ecology, 97(1), 67-77.

Chmura, G. L., Anisfeld, S. C., Cahoon, D. R., & Lynch, J. C. (2003). Global carbon sequestration in tidal, saline wetland soils. Global biogeochemical cycles, 17(4).

Dariah, A., Marwanto, S., & Agus, F. (2014). Root-and peat-based CO2 emissions from oil palm plantations. Mitigation and Adaptation Strategies for Global Change, 19(6), 831-843.

Day, J. W., Rismondo, A., Scarton, F., Are, D., & Cecconi, G. (1998). Relative sea level rise and Venice lagoon wetlands. Journal of Coastal Conservation, 4(1), 27-34.

Esri ArgGIS Pro Help LAS Dataset toolset, http://www.arcgis.com; (accessed November 2021)

Flowers, T. J. (1985). Physiology of halophytes. In Biosalinity in action: bioproduction with saline water (pp. 41-56). Springer, Dordrecht.

Flowers, T. J., Galal, H. K., & Bromham, L. (2010). Evolution of halophytes: multiple origins of salt tolerance in land plants. Functional Plant Biology, 37(7), 604-612.

Flowers, T. J., Hajibagheri, M. A., & Clipson, N. J. W. (1986). Halophytes. The quarterly review of biology, 61(3), 313-337.

Friedrichs, C. T., & Perry, J. E. (2001). Tidal salt marsh morphodynamics: a synthesis. Journal of Coastal Research, 7-37.

Holmquist, J. R., Windham-Myers, L., Bernal, B., Byrd, K. B., Crooks, S., Gonneea, M. E., ... & Weller, D. E. (2018). Uncertainty in United States coastal wetland greenhouse gas inventorying. Environmental Research Letters, 13(11), 115005.

Houldcroft, C. J., Campbell, C. L., Davenport, I. J., Gurney, R. J., & Holden, N. (2005). Measurement of canopy geometry characteristics using LiDAR laser altimetry: A

`
feasibility study. IEEE Transactions on Geoscience and Remote Sensing, 43(10), 2270-2282.

James, M.R., Robson, S., (2012) Straightforward reconstruction of 3D surfaces and topography with a camera: accuracy and geoscience application. J. Geophys. Res. 117.

Jennings, D. H. (1968). Halophytes, succulence and sodium in plants—a unified theory. New Phytologist, 67(4), 899-911.

Kerle, N., Janssen, L. L., & Huurneman, G. C. (2004). Principles of remote sensing. ITC, Educational textbook series, 2, 250.

Kirwan, M. L., & Murray, A. B. (2007). A coupled geomorphic and ecological model of tidal marsh evolution. Proceedings of the National Academy of Sciences, 104(15), 6118-6122.

Kirwan, M. L., Guntenspergen, G. R., d'Alpaos, A., Morris, J. T., Mudd, S. M., & Temmerman, S. (2010). Limits on the adaptability of coastal marshes to rising sea level. Geophysical research letters, 37(23).

LAS 1.4 format specification, Technical Report, The American Society for Photogrammetry & Remote Sensing, (2011) http://www.asprs.org/a/society/committees/standards/LAS_1_4_r13.pdf (accessed 20 may 2022)

LAS format specifications for ver. 1.2., 2 September 2008. https://www.asprs.org/a/society/committees/standards/asprs_las_format_v12.pdf (accessed 20 May 2022)

Lefsky, M. A., Cohen, W. B., Parker, G. G., & Harding, D. J. (2002). Lidar remote sensing for ecosystem studies: Lidar, an emerging remote sensing technology that directly measures the three-dimensional distribution of plant canopies, can accurately estimate vegetation structural attributes and should be of particular interest to forest, landscape, and global ecologists. BioScience, 52(1), 19-30.

Lowe, D.G., 2004. Distinctive image features from scale-invariant keypoints. Int. J. Comput. Vis. 60 (2), 91–110.

`

Marani, M., Silverstri, S., Belluco, E., Camuffo, M., D'Alpaos, A., Lanzoni, S., ... & Rinaldo, A. (2003, July). Patterns in tidal environments: salt-marsh channel networks and vegetation. In IGARSS 2003. 2003 IEEE International Geoscience and Remote Sensing Symposium. Proceedings (IEEE Cat. No. 03CH37477) (Vol. 5, pp. 3269-3271). IEEE.

Mcleod, E., Chmura, G. L., Bouillon, S., Salm, R., Björk, M., Duarte, C. M., ... & Silliman, B. R. (2011). A blueprint for blue carbon: toward an improved understanding of the role of vegetated coastal habitats in sequestering CO2. Frontiers in Ecology and the Environment, 9(10), 552-560.

NSF (2019) Coupled ecological-geomorphological response of coastal wetlands to environmental change - Project description

Odum E. P.(1971) Fundamentals of Ecology, 3rd ed., W. B. Sanders College Pub., Philadelphia (pp. 544)

Pendleton, L., Donato, D. C., Murray, B. C., Crooks, S., Jenkins, W. A., Sifleet, S., ... & Baldera, A. (2012). Estimating global “blue carbon” emissions from conversion and degradation of vegetated coastal ecosystems.

Pethick, J. (1984). An introduction to Coastal Geomorphology,(pp. 73-74) Arnold Pub.

Rapidlasso LASTools http://rapidlasso.com/ (Accessed 02 February 2022).

Remondino, F., Spera, M.G., Nocerino, E., Menna, F., Nex, F., 2014. State of the art in high density image matching. Photogramm. Rec. 29 (146), 144–166.

Riley, D., & Barber, S. A. (1970). Salt Accumulation at the Soybean (Glycine Max.(L.) Merr.) Root-Soil Interface. Soil Science Society of America Journal, 34(1), 154-155.

Silvestri, S., & Marani, M. (2004). Salt-marsh vegetation and morphology: Basic physiology, modelling and remote sensing observations. The Ecogeomorphology of Tidal Marshes, Coastal Estuarine Stud, 59, 5-25.

Silvestri, S., Defina, A., & Marani, M. (2005). Tidal regime, salinity and salt marsh plant zonation. Estuarine, coastal and shelf science, 62(1-2), 119-130.

`

Silvestri, S., Marani, M., & Marani, A. (2003). Hyperspectral remote sensing of salt marsh vegetation, morphology and soil topography. Physics and Chemistry of the Earth, Parts a/B/C, 28(1-3), 15-25.

Silvestri, S., Marani, M., Settle, J., Benvenuto, F., & Marani, A. (2002). Salt marsh vegetation radiometry: Data analysis and scaling. Remote Sensing of Environment, 80(3), 473-482.

Snavely, N., Seitz, S.M., Szeliski, R., 2006. Photo tourism: exploring photo collections in 3D.ACMTrans. Graph. 25 (3), 835–846.

Syvitski, J. P., Vorosmarty, C. J., Kettner, A. J., & Green, P. (2005). Impact of humans on the flux of terrestrial sediment to the global coastal ocean. science, 308(5720), 376-380.

Temmerman, S., Meire, P., Bouma, T. J., Herman, P. M., Ysebaert, T., & De Vriend, H. J. (2013). Ecosystem-based coastal defence in the face of global change. Nature, 504(7478), 79-83.

Visser, E. J. W., Colmer, T. D., Blom, C. W. P. M., & Voesenek, L. A. C. J. (2000). Changes in growth, porosity, and radial oxygen loss from adventitious roots of selected mono-and dicotyledonous wetland species with contrasting types of aerenchyma. Plant, Cell & Environment, 23(11), 1237-1245.

Wang, C., Menenti, M., Stoll, M. P., Belluco, E., & Marani, M. (2007). Mapping mixed vegetation communities in salt marshes using airborne spectral data. Remote Sensing of Environment, 107(4), 559-570.

World Water Assessment Programme (United Nations). (2003). Water for People, Water for Life: A Joint Report by the Twenty-three UN Agencies Concerned with Freshwater. UNESCO Pub.

Yang, Z., D’Alpaos, A., Marani, M., & Silvestri, S. (2020). Assessing the fractional abundance of highly mixed salt-marsh vegetation using random forest soft classification. Remote Sensing, 12(19), 3224.

Yousefi Lalimi, F., & Marani, M. (2016). Organic matter and decomposition rate observational data from salt marshes of North Carolina.

`

Zedler, J. B., Bonin, C. L., Larkin, D. J., & Varty, A. (2018). Salt marshes. In Encyclopedia of ecology (pp. 614-622). Elsevier.

Zhang, K., Chen, S. C., Whitman, D., Shyu, M. L., Yan, J., & Zhang, C. (2003). A progressive morphological filter for removing nonground measurements from airborne LIDAR data. IEEE transactions on geoscience and remote sensing, 41(4), 872-882.

`

6 APPENDIX

6.1 List of the materials taken on the field campaign

List of materials to take to the field		
Material	**Quantity**	**Observations**
PVC joints*	8	
PVC piping	8 m	
DGPS	1	RTK correction
Tape measure	2	at least 2 meters long
Knives	2	
Scale	2	
20x20 cm quadrat	2	
Plastic bags	~400	Sometimes 2 per sample is needed
Paper bags	~200	
10 cm by 30 cm PVC	2	
Aluminum trays	30	
Pestle	1	
1 mm sieve	1	
500 microns sieve	1	
Notebook	2	At least 2, it is very important to take very good notes
Pens	5	
Permanent marker	5	To write the names on the plastic bags
Cellphone/Camera	2	To take a good picture of the plots
Gloves	6	Those used by doctors are comfortable but break a lot, those used for washing dishes are resistant but not very comfortable in the field.
Rubber hammer	1	
Wooden tray	2	To cut the 30 cm long sediment samples, they should be large enough
Bricklayer's trowel (see image)	1	
Impermeable layer (for picnic)	2	Impervious fabrics to be used as a base for materials during work
Big thermal bags	10	Sediments should be protected from heat after collection so that they do not melt
Pvc pipe covers (see image)		For the sediment suction to be performed, it is necessary that the pcv pipes are plugged, we use a piece of

`

		paper and adhesive tape to improve the vacuum effect.
Paper tape	2	
Kitchen paper	4	For cleaning the materials after using, to prevent contaminations from plot to plot
Scissors	2	
Long rubber boots		Everyone must have it
Drone with camera		
Drone with hyperspectral		
Drone with hyperspectral laser scanner (for Lidar)		
Targets		For ground point corrections
Small saw	1	For cutting vegetation
hand pruners	1	
Semi-rigid meter	2	For delineate the 1m x 1 m plot
Plastic tape (transparent)	2	

6.2 Data collected of each plot by observations done on the field

Estimation of Vegetation Cover – Plot 2	
Cover	**Percentage (%)**
Limonium	80
Sarcocornia	20

Vegetation Height (cm) – Plot 2	
Corner 1	10
Corner 2	11
Corner 3	36
Corner 4	42
Center	37

Plot 2 - Picture


Estimation of Vegetation Cover – Plot 3	
Cover	**Percentage (%)**
Soil	50
Salicornia	50

Vegetation Height (cm) – Plot 3	
Corner 1	20
Corner 2	22
Center	23

Plot 3- Picture
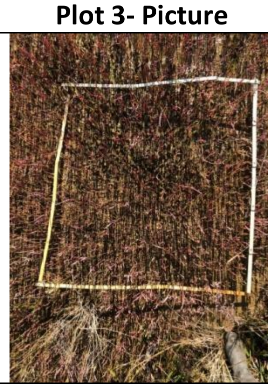

Estimation of Vegetation Cover – Plot 4	
Cover	**Percentage (%)**
Spartina Anglica	90
Salicornia	10

Vegetation Height (cm) – Plot 4	
Corner 1	59
Corner 2	20
Center	18

`

Plot 4 - Picture


Estimation of Vegetation Cover – Plot 5	
Cover	**Percentage (%)**
Limonium	80
Sarcocornia	15
Soil	5

Vegetation Height (cm) – Plot 5	
Corner 1	28
Corner 2	18
Corner 3	12
Corner 4	17
Center	21

Plot 5 - Picture


Estimation of Vegetation Cover – Plot 6	
Cover	**Percentage (%)**
Spartina Anglica	90
Soil	10

`

Vegetation Height (cm) – Plot 6	
Corner 1	14
Corner 2	30
Corner 3	34
Corner 4	20
Center	17

Plot 6 - Picture

Estimation of Vegetation Cover – Plot 7	
Cover	**Percentage (%)**
Spartina Maritima	50
Limonium	30
Soil	20

Vegetation Height (cm) – Plot 7	
Corner 1	22
Corner 2	16
Corner 3	27
Corner 4	30
Center	26

Plot 7 - Picture

Estimation of Vegetation Cover – Plot 8	
Cover	**Percentage (%)**
Sarcocornia	100

Vegetation Height (cm) – Plot 8	
Corner 1	17
Corner 2	25
Corner 3	23
Corner 4	10
Center	14

Plot 8 - Picture


Estimation of Vegetation Cover – Plot 9	
Cover	**Percentage (%)**
Salicornia	40
Soil	60

Vegetation Height (cm) – Plot 9	
Corner 1	29
Corner 2	16
Corner 3	17
Corner 4	18
Center	26

`

Plot 9 - Picture


Estimation of Vegetation Cover – Plot 10	
Cover	**Percentage (%)**
Inula	60
Sarcocornia	25
Juncus	10
Limonium	5

Vegetation Height (cm) – Plot 10	
Corner 1	59
Corner 2	80
Corner 3	45
Corner 4	50
Center	39

Plot 10 - Picture


`

6.3 Step by step procedure for the soil organic carbon though LOI analysis

What to do	Things to pay attention
1) Turn on the furnace and set it to about 90-100 ° C.	- The furnace must be in manual mode (white button)
2) Put 6 crucibles to dry in the furnace for about 30 min	
3) Put the crucibles in the dryer, one by one. Wait long enough for them to return to room temperature (i.e. don't weigh them when hot)	- Check that the salts in the dryer are blue and not pink (otherwise they are no longer able to absorb humidity) - Touch the crucibles with tongs or gloves to prevent humidity transfer
4) Weigh a crucible and note the tare weight	- Remember to close all the doors of the scale and wait for the unit of measurement to appear - Touch the crucibles with tongs or gloves to prevent humidity transfer
5) Put a few spoons of sample in the crucible, be sure that there are about 7-8 grams	- Remember to mix the sample well before placing it in the crucible. It must be as representative as possible
6) Write the name of the sample on the crucible	- Use permanent markers
7) Put the crucible with the sample inside to dry in the furnace (always at about 90-100 ° C) for about 1 hour	
8) Repeat steps 4-7 for all crucibles	- Touch the crucibles with tongs or gloves to prevent humidity transfer
9) Put the crucibles + sample in the dryer, one at a time. Wait long enough for them to return to room temperature (i.e. don't weigh them hot)	- Touch the crucibles with tongs or gloves to prevent humidity transfer
10) Weigh a crucible + sample and note the weight	- Remember to close all the doors of the scale and wait for the unit of measurement to appear - Touch the crucibles with tongs or gloves to prevent humidity transfer
11) Put the crucible + sample in the furnace and note the position on a sheet	- Drawing like a map of the positions of each one
12) Repeat operations 9-11 for all crucibles	
13) Be sure that the furnace is switched on at 100 ° C , set it manually. Wait 1 hour and then go to raise the temperature by 100 ° C. After 1 hour another 100 ° C. Keep going until it reaches 450 ° C.	
14) Now the furnace must be set to run automatic mode:	- The red and green plastics are very delicate and are the last we have. Please be careful.

- Red plastic = start; green plastic = stop. Set it to turn off 8 hours after you put it at 450 ° C. - turn the clock clockwise until the red plastic passes the white dot at the top right (you have to feel that it overcomes a certain resistance to rotation, then it's ok) - To set the furnace in automatic mode use the white button	
After 8 hours have passed, wait another 8 hours before handling the samples again	
15) Write the sample name map on the table, in order to position the samples in the same order in which they were placed in the furnace, after many hours at high temperatures, the name written on the crucible will have disappeared	- At least 8 hours must have passed since the furnace was switched off
16) Take out one crucible at a time using the pincers	- Close the furnace immediately - Touch the crucibles with the tongs so as not to transfer humidity; do not touch them with gloves as they will probably be hot.
17) Write the name on the crucible and put it in the dryer. Wait long enough for them to return to room temperature (i.e. don't weigh them hot)	- Touch the crucibles with the tongs so as not to transfer humidity; do not touch them with gloves as they will probably be hot.
18) Weigh a crucible + sample and note the weight	- Remember to close all the doors of the scale and wait for the unit of measurement to appear - Touch the crucibles with tongs or gloves to prevent humidity transfer
19) Washing: - crucibles with normal water and then with distilled water - clean the table with acetone	
Timing: - Point 12 must be completed by 15:00 at the latest so that 450 ° C is reached at the latest by 18:30. After 18:30 it is not allowed to be at the laboratory. It can take up to 3.5-4 hours to do points 1 to 12. If you want to bake other samples the next day (considering the 8 hours in which the furnace must cool + the weighing time + the crucible washing time) The recommendation is to start at 9 o'clock or at the latest 10 o'clock.	

`

6.4 Calculation of the aboveground dry biomass (g/m2)

Aboveground dry biomass									
	Sample Name	Date of sampling	Weight of the sample when humid (g)	Weight of the bag when humid (g)	Weight of the bag + sample when humid (g)	Weight of the bag + sample when dry (g)	Weight of the bag when dry (g)	Weight of the sample when dry(g)	Aboveground dry biomass (g/m2)
1	P1B1	September 9th	36.00	11.07	25.29	22.44	10.46	11.98	299.50
2	P1B2	September 9th	44	12.82	28.80	26.73	12.42	14.31	357.75
3	P1B3	September 9th	34	10.06	23.34	21.69	9.77	11.92	298.00
4	P2B1	September 9th	60.00	12.15	37.04	33.33	11.50	21.83	545.75
5	P2B2	September 9th	48	11.99	29.42	27.41	11.61	15.80	395.00
6	P2B3	September 9th	86	11.99	32.64	30.37	11.79	18.58	464.50
7	P3B1	September 10th	38	9.37	16.47	15.33	9.25	6.08	152.00
8	P3B2	September 9th	34.00	9.97	17.65	15.26	9.49	5.77	144.25
9	P3B3	September 10th	62.00	11.24	26.41	20.26	10.77	9.49	237.25
10	P4B1	September 10th	64	14.88	36.70	33.8	14.55	19.25	481.25
11	P4B2	September 10th	54	10.99	27.28	25.27	10.64	14.63	365.75
12	P4B3	September 10th	46.00	10.75	26.26	22.77	10.15	12.62	315.50
13	P5B1	September 10th	72	13.17	39.64	36.63	13.06	23.57	589.25
14	P5B2	September 10th	78	11.22	35.28	32.07	10.91	21.16	529.00
15	P5B3	September 10th	58.00	11.28	35.70	31.89	10.77	21.12	528.00
16	P6B1	September 10th	48	10.70	24.41	22.21	10.33	11.88	297.00
17	P6B2	September 10th	50.00	11.40	27.17	23.58	11.10	12.48	312.00
18	P6B3	September 10th	64.00	11.50	31.47	27.51	10.98	16.53	413.25
19	P7B1	September 10th	42	10.83	26.25	23.89	10.61	13.28	332.00
20	P7B2	September 10th	52.00	12.33	30.88	27.45	11.91	15.54	388.50
21	P7B3	September 10th	24	9.28	17.96	16.65	9.08	7.57	189.25
22	P8B1	September 10th	166	15.20	73.66	66.08	14.85	51.23	1280.75
23	P8B2	September 10th	84	15.11	48.61	44.45	14.87	29.58	739.50
24	P8B3	September 10th	188.00	20.43	98.56	80.60	19.77	60.83	1520.75
25	P9B1	September 10th	54.00	10.67	28.43	18.90	10.06	8.84	221.00
26	P9B2	September 10th	44	9.97	18.43	16.93	9.82	7.11	177.75
27	P9B3	September 10th	21.00	11.04	15.61	13.38	10.57	2.81	70.25
28	P10B1	September 12th	130	20.71	87.57	80.43	20.58	59.85	1496.25
29	P10B2	September 10th	66.00	13.33	47.39	36.58	13.02	23.56	589.00

`

30	P10B3	September 12th	32	9.94	19.71	17.34	9.69	7.65	191.25
31	1	September 13th	124.00	13.09	97.66	33.66	12.60	21.06	526.50
32	2	September 13th	56.00	10.65	33.19	25.75	10.23	15.52	388.00
33	3	September 13th	22.00	9.84	17.50	12.05	9.35	2.70	67.50
34	4	September 13th	46.00	9.75	28.14	16.21	9.14	7.07	176.75
35	5	September 13th	66.00	10.66	40.05	19.78	10.31	9.47	236.75
36	6	September 13th	120.00	13.47	99.58	54.40	13.21	41.19	1029.75
37	7	September 13th	36.00	10.86	25.48	15.50	10.43	5.07	126.75
38	8	September 13th	78.00	13.59	71.09	41.44	13.16	28.28	707.00
39	9	September 13th	62.00	10.59	34.66	25.53	10.14	15.39	384.75
40	10	September 13th	32	11.27	23.20	20.27	10.98	9.29	232.25
41	11	September 13th	44.00	10.98	35.59	26.27	10.40	15.87	396.75
42	12	September 13th	50.00	12.07	37.52	30.60	11.53	19.07	476.75
43	13	September 13th	62.00	10.18	44.51	30.72	9.87	20.85	521.25
44	14	September 13th	48.00	12.00	35.93	25.93	11.53	14.40	360.00
45	15	September 13th	234.00	15.19	168.35	106.52	14.64	91.88	2297.00
46	16	September 13th	128.00	20.83	97.98	82.31	20.04	62.27	1556.75
47	17	September 13th	162.00	20.53	126.00	71.25	19.69	51.56	1289.00
48	18	September 13th	72	14.56	54.42	44.89	14.24	30.65	766.25
49	19	September 13th	122.00	14.12	111.85	47.60	13.48	34.12	853.00
50	20	September 13th	34.00	9.75	27.03	20.53	9.38	11.15	278.75
51	21	September 13th	106	15.30	63.42	55.06	14.94	40.12	1003.00
52	22	September 13th	54.00	14.77	44.51	34.00	14.21	19.79	494.75
53	23	September 13th	136.00	20.59	94.79	58.64	19.93	38.71	967.75
54	24	September 13th	182.00	20.62	132.78	73.53	19.78	53.75	1343.75
55	25	September 13th	274.00	20.62	183.81	114.56	19.44	95.12	2378.00

`

6.5 Calculation of bulk density

Bulk Density											
				Volume of the cylinder (cm3) --> 785							
	Name of samples	**Foil recipient (g)**	**Recipient with sample (g)**	**Weight 1 (g)**	**Weight 2 (g)**	**Weight 3 (g)**	**Weight 4 (g)**	**Weight 5 (g)**	**Weight 6 (g)**	**Bulk density (g/cm3)**	**Bulk density (g/m2(**
1	P1B1	8.72	970.2	641.3	498.6	472.1	469.5			0.59	5870.2
2	P1B2	8.70	902.8	507.5	378.6	372.7	371.9			0.46	4626.9
3	P1B3	8.73	896.6	575.3	414.4	398.0	398.0			0.50	4958.3
4	P2B1	13.45	911.1	448.7	415.6	414.8	414.0			0.51	5102.7
5	P2B2	10.86	977.6	540.1	512.2	511.4	510.7			0.64	6366.8
6	P2B3	8.74	876.7	460.0	389.0	388.4	388.0			0.48	4831.0
7	P3B1	13.64	910.9	415.9	398.8	397.8	397.0			0.49	4883.1
8	P3B2	8.65	864.6	401.6	393.6	392.4	390.9			0.49	4869.0
9	P3B3	13.68	908.1	392.5	388.6	387.7	386.6			0.48	4750.8
10	P4B1	11.05	821.9	441.0	312.7	311.2	310.8			0.38	3818.5
11	P4B2	13.18	820.1	404.3	323.1	322.4	322.3			0.39	3937.7
12	P4B3	10.90	834.3	497.5	344.4	339.7	339.4			0.42	4184.8
13	P5B1	8.96	891.4	429.4	360.0		359.2			0.45	4461.0
14	P5B2	8.94	863.2	405.2	358.4		358.0			0.44	4446.4
15	P5B3	8.9	760.3	338.5	295.4		295.0			0.36	3644.6
16	P6B1	13.13	1070.2	1003.0	692.9	612.0	493.6	492.4	492.1	0.61	6101.4
17	P6B2	15.89	932.6	811.1	496.5	437.0	404.1	404.0	403.8	0.49	4941.5
18	P6B3										
19	P7B1	13.20	908.6	794.3	447.2	372.8	309.5	309.2	308.8	0.38	3766.1
20	P7B2	13.22	885.8	748.7	392.9	344.5	322.6	322.5	322.3	0.39	3937.1
21	P7B3	8.88	863.2	402.0	307.5				307.0	0.38	3798.1
22	P8B1	8.97	900.7	461.4	369.5				369.0	0.46	4586.5
23	P8B2	13.23	892.1	800.7	500.0	447.4	420.0	419.6	419.2	0.52	5172.1
24	P8B3	10.96	911.4	413.8	391.6				390.5	0.48	4835.2
25	P9B1	8.62	864.5	790.9	490.1	431.2	408.1	408.0	407.9	0.51	5086.9
26	P9B2	8.64	342.5	299.7	263.3	263.1	262.8	262.7	262.7	0.32	3236.3
27	P9B3										
28	P10B1	15.83	848.2	788.4	535.5	488.6	459.6	459.3	459.1	0.56	5646.5
29	P10B2										
30	P10B3	8.64	979.9	897.1	626.2	582.4	671.5	571.5	571.4	0.72	7168.7

`

6.6 Calculation of soil organic carbon though LOI

Soil organic carbon though Loss of Ignition (LOI)									
	Name	Crucible weight (g)	Sample weight organic matter + inorganic matter (g)	Sample weight organic matter + inorganic matter + crucible after 1h (g)	Sample weight organic matter + inorganic matter after 1h (g)	Sample weight inorganic matter + crucible (g)	Sample weight inorganic matter (g)	Ashes (%)	LOI (= % O.M.)
1	P1B1	71.80	9.51	81.25	9.45	79.93	8.13	86.05	13.95
2	P1B2	54.67	7.31	61.96	7.28	60.81	6.14	84.29	15.71
3	P1B3	55.09	7.20	62.24	7.15	61.07	5.98	83.65	16.35
4	P2B1	71.81	8.42	80.14	8.33	78.88	7.07	84.93	15.07
5	P2B2	71.80	7.21	78.96	7.16	78.20	6.40	89.38	10.62
6	P2B3	57.52	7.84	65.28	7.77	64.14	6.62	85.29	14.71
7	P3B1	55.29	7.62	62.87	7.59	61.97	6.68	88.08	11.92
8	P3B2	56.07	7.52	63.55	7.49	62.66	6.59	88.07	11.93
9	P3B3	57.51	7.49	64.96	7.45	63.82	6.31	84.72	15.28
10	P4B1	57.51	7.40	64.87	7.36	64.84	7.32	99.51	0.488
11	P4B2	57.51	7.77	65.24	7.72	64.10	6.58	85.25	14.75
12	P4B3	57.51	7.56	65.05	7.54	63.91	6.40	84.83	15.17
13	P5B1	55.29	5.61	60.85	5.56	59.81	4.52	81.32	18.68
14	P5B2	57.52	6.36	63.85	6.33	62.92	5.41	85.42	14.58
15	P5B3	81.42	7.60	88.97	7.55	87.81	6.39	84.65	15.35
16	P6B1	55.28	8.44	63.70	8.41	62.77	7.49	89.03	10.97
17	P6B2	57.51	7.04	64.51	7.00	63.64	6.12	87.48	12.52
18	P6B3								
19	P7B1	71.80	9.17	80.90	9.10	79.39	7.58	83.37	16.63
20	P7B2	57.51	7.42	64.89	7.38	63.61	6.09	82.58	17.42
21	P7B3	56.08	7.22	63.25	7.17	62.68	6.60	92.02	7.98
22	P8B1	54.67	6.34	60.97	6.30	60.01	5.34	84.72	15.28
23	P8B2	55.28	7.93	63.19	7.90	62.22	6.94	87.83	12.17
24	P8B3	56.07	6.19	62.21	6.14	61.40	5.33	86.77	13.23
25	P9B1	71.81	8.18	79.58	7.77	79.23	7.42	95.51	4.49
26	P9B2	71.81	9.24	81.02	9.21	80.72	8.91	96.76	3.24
27	P9B3								
28	P10B1	71.81	6.62	78.39	6.58	77.62	5.81	88.21	11.79
29	P10B2								
30	P10B3	55.09	6.48	61.55	6.46	60.94	5.85	90.59	9.41

`

6.7 Calculation of the belowground biomass (g/m2)

Belowground for dry biomass analysis (g/m2)															
	Name	Part	Observations	Height (cm)	Base area (cm2)	Volume (cm3)	Tare weight - aluminum tray (g)	Aluminum tray + sample when humid (g)	Aluminum tray + sample when dry (g)				Below-ground biomass (g)	Below-ground biomass (g/m2)	Below-ground biomass weight (g/m^2) in 10 cm of depth
1	P1B1	1st		10	78.5	785	8.84	215.66	48.51	31.61	31.59		22.75	289.81	2898.09
2	P1B2	1st		10	78.5	785	11.03	226.26	50.50	36.20	36.14	32.14	21.11	268.92	2689.17
3	P1B3	1st		10	78.5	785	16.38	298.31	80.89	47.87	47.79		31.41	400.13	4001.27
4	P2B1	1st		10	78.5	785	11.12	240.93	44.48	37.34			26.22	334.01	3340.13
5	P2B2	1st		10	78.5	785	6.84	235,19	79.39	37.15			30.31	386.11	3861.15
6	P2B3	1st		10	78.5	785	6.05	156.87	37.15	21.16	21.00		14.95	190.45	1904.46
7	P3B1	1st		10	78.5	785	5.76	112.46	16.27	16.15	16.09		10.33	131.59	1315.92
8	P3B2	1st		10	78.5	785	5.98	89.83	15.38	13.01	12.96		6.98	88.92	889.17
9	P3B3	1st		10	78.5	785	5.62	144.08	24.73	17.24	17.13		11.51	146.62	1466.24
10	P4B1	1st		10	78.5	785	16.24	193.93	34.37	32.27	31.72	31.66	15.42	196.43	1964.33
11	P4B2	1st		10	78.5	785	10.97	158.10	82.29	57.90	22.00	21.95	10.98	139.87	1398.73
12	P4B3	1st		10	78.5	785	10.99	167.98	88.96	45.19	26.05	26.02	15.03	191.46	1914.65
13	P5B1	1st	0-10 cm	10	50.24	502.4	8.81	164.2	35.27	34.64	34.42		25.61	509.75	5097.53
14	P5B1	2nd	10-20 cm	10	50.24	502.4	6.75	101.95	21.24	21.11	21.03		14.28	284.24	2842.36
15	P5B1	3rd	20-30 cm	10	50.24	502.4	8.92	42.76	14.18	14.17	14.13		5.21	103.70	1037.02
16	P5B2	1st	0-10 cm	10	50.24	502.4	7.66	100.75	18.8	18.76			11.10	220.94	2209.39
17	P5B2	2nd	10-20 cm	10	50.24	502.4	6.83	72.91	18.04	17.98			11.15	221.93	2219.35
18	P5B2	3rd	20-30 cm	10	50.24	502.4	7.55	36.68	10.22	10.17			2.62	52.15	521.50
19	P5B3	1st	0-10 cm	10	50.24	502.4	5.82	123.21	27.71	26.93			21.11	420.18	4201.83
20	P5B3	2nd	10-20 cm	10	50.24	502.4	6.45	69.88	16.57	16.52			10.07	200.44	2004.38
21	P5B3	3rd	20-30	10	50.24	502.4	6.95	28.39	8.32	8.29			1.34	26.67	266.72
22	P6B1	1st		10	50.24	502.4	5.92	67.03	11.10	11.11	11.17		5.18	103.11	1031.05
23	P6B1	2nd		10	50.24	502.4	6.66	42.97	10.10	10.10	10.12		3.44	68.47	684.71
24	P6B1	3rd													
25	P6B2	1st		10	50.24	502.4	5.76	71.12	10.95				5.19	103.30	1033.04
26	P6B2	2nd		10	50.24	502.4	6.26	41.89	7.69				1.43	28.46	284.63
27	P6B2	3rd													
28	P6B3	1st		10	50.24	502.4	10.85	68.96	14.44	14.39	14.45		3.54	70.46	704.62
29	P6B3	2nd		10	50.24	502.4	16.05	53.25	20.85	20.86	20.92		4.80	95.54	955.41
30	P6B3	3rd		10	50.24	502.4	10.86	21.78	11.75	11.76	11.80		0.89	17.71	177.15
31	P7B1	1st		10	50.24	502.4	6.4	176.99	25.88	25.84	25.88		19.44	386.94	3869.43
32	P7B1	2nd		10	50.24	502.4	6.42	70.1	13.1	12.98	13.03		6.56	130.57	1305.73

`

33	P7B1	3rd	20-29 cm	9	50.24	452.16	6.31	26.65	7.82	7.81	7.84		1.50	33.17	331.74
34	P7B2	1st		10	50.24	502.4	5.85	110.48	76.2	40.93	17.07		11.22	223.33	2233.28
35	P7B2	2nd		10	50.24	502.4	6.88	74.47	32.84	16.21	15.57		8.69	172.97	1729.70
36	P7B2	3rd		10	50.24	502.4	6.39	36.83	10.67	9.88	9.77		3.38	67.28	672.77
37	P7B3	1st		10	50.24	502.4	6.28	193.18	21.47	21.45	21.45		15.17	301.95	3019.51
38	P7B3	2nd		10	50.24	502.4	5.91	64.17	11.03	11.03	11.04		5.12	101.91	1019.11
39	P7B3	3rd		10	50.24	502.4	7.07	38.36	8.71	8.71	8.73		1.64	32.64	326.43
40	P8B1	1st	0-10 cm	10	50.24	502.4	7.16	104.85	21.78	21.17			14.01	278.86	2788.61
41	P8B1	2nd	10-20 cm	10	50.24	502.4	6.94	59.23	13.75	13.72			6.78	134.95	1349.52
42	P8B1	3rd	20-28 cm	8	50.24	401.92	6.42	28.76	9.94	9.92			3.50	87.08	870.82
43	P8B2	1st		10	50.24	502.4	5.84	101.19	11.10				5.26	104.70	1046.97
44	P8B2	2nd	10-20 cm	10	50.24	502.4	6.31	82.7	42.11	19.6	16.65		10.34	205.81	2058.12
45	P8B2	3rd	20-29 cm	9	50.24	452.16	6.77	48.67	17.38				10.61	234.65	2346.51
46	P8B3	1st	0-10 cm	10	50.24	502.4	6.11	235.46	32.10	32.04			25.93	516.12	5161.23
47	P8B3	2nd		10	50.24	502.4	6.8	82.53	49.68	29.64	14.8		8.00	159.24	1592.36
48	P8B3	3rd	20-24.5 cm	4.5	50.24	226.08	5.68	25.91	10.12	10.14	10.12		4.44	196.39	1963.91
49	P9B1	1st													
50	P9B1	2nd													
51	P9B1	3rd													
52	P9B2	1st		10	50.24	502.4	6.57	14.14	13.1	13.08	13.07		6.50	129.38	1293.79
53	P9B2	2nd	10-20 cm	10	50.24	502.4	5.85	22.11	8.62	8.6	8.59		2.74	54.54	545.38
54	P9B2	3rd		10	50.24	502.4							0.00	0.00	0.00
55	P9B3	1st		10	50.24	502.4	5.65	19.15	8.75	8.74	9.69		3.09	61.50	615.05
56	P9B3	2nd													
57	P9B3	3rd													
58	P10B1	1st	0-10 cm	10	50.24	502.4	6.62	102.92	20.72	20.16			13.54	269.51	2695.06
59	P10B1	2nd		10	50.24	502.4	6.11	91.46	12.24	12.25	12.27		6.13	122.01	1220.14
60	P10B1	3rd	20-28 cm	8	50.24	401.92	6.18	41.89	13.38	9.8	9.66		3.48	86.58	865.84
61	P10B2	1st		10	50.24	502.4	6.2	69.13	42.42	19.74	18.3		12.10	240.84	2408.44
62	P10B2	2nd		10	50.24	502.4	5.8	39.73	10.63	10.57	10.56		4.76	94.75	947.45
63	P10B2	3rd		10	50.24	502.4	6.00	26.71	8.45	8.46	8.44		2.44	48.57	485.67
64	P10B3	1st		10	50.24	502.4	5.85	81.54	14.97	14.9	14.85		9.00	179.14	1791.40
65	P10B3	2nd		10	50.24	502.4	6.76	43.1	13.14	11.07	11.02		4.26	84.79	847.93
66	P10B3	3rd													

6.8 Summary of the results obtained by using Excel spreadsheets for LiDAR and DSM

Name	Zmax/With Outliers (m)	Zmin/With Outliers (m)	Cloud Thickness (m)/With Outliers	Point Count LiDAR/ With Outliers	Zmax/Without Outlier (m)	Zmin/Without Outlier (m)	Cloud Thickness/Without Outlier (m)	Point Count LiDAR/ Without Outliers	GNSS Point Z (m)	Average Z / DSM	Average Z/ With Outliers (m)	Average Z/ Without Outliers (m)	Z Variation/ With Outliers (m)	Z Variation/ Without Outliers (m)	Scan Angle /Average	Standard Deviation / DSM	Standard Deviation / Lidar	Max Vegetation Height/ Measured (m)	Average Vegetation Height/ Measured (m)
Control 1 / Target 1	0.49	-0.02	0.51	41	0.49	0.34	0.15	40	0.35	0.39	0.40	0.41	-0.05	-0.06	7	0.010	0.036		
Control 2 / Target 2	0.53	0.35	0.19	33	0.53	0.43	0.10	29	0.39	0.40	0.49	0.49	0.01	0.00	12	0.010	0.039		
Control 3 / Target 3	0.49	0.31	0.19	61	0.45	0.34	0.10	58	0.41	0.43	0.40	0.40	0.01	0.01	-6	0.003	0.025		
Control 4 / Target 4	0.53	0.35	0.19	61	0.53	0.43	0.10	58	0.49	0.42	0.49	0.49	0.01	0.00	4	0.005	0.026		
Control 5 / Target 5	0.59	0.43	0.17	70	0.59	0.45	0.14	68	0.47	0.45	0.52	0.53	-0.06	-0.06	-2	0.004	0.031		
Control 6 Target 6	0.50	0.33	0.17	71	0.50	0.39	0.11	68	0.40	0.41	0.43	0.44	-0.04	-0.04	-5	0.017	0.024		
Control 7 / Target 7	0.58	0.43	0.15	40	0.58	0.43	0.15	40	0.50	0.50	0.51	0.51	-0.01	-0.01	-9	0.006	0.040		
Control 8 / Target 8	0.49	0.37	0.11	45	0.49	0.37	0.11	45	0.39	0.44	0.42	0.42	-0.03	-0.03	-9	0.006	0.027		
Control 9 Target 9	0.44	0.21	0.23	36	0.44	0.31	0.13	33	0.36	0.30	0.38	0.38	-0.03	-0.04	18	0.007	0.032		
Control 10 / Target 10	0.40	0.31	0.40	28	0.40	0.13	0.27	25	0.32	0.42	0.26	0.26	0.06	0.05	18	0.018	0.057		
Control 11 / Target 11	0.31	0.06	0.24	39	0.27	0.06	0.21	38	0.15	0.17	0.17	0.17	-0.02	-0.02	20	0.007	0.044		
Control 12 Target 12	0.37	0.27	0.10	26	0.35	0.30	0.04	21	0.30	0.38	0.32	0.32	-0.02	-0.02	-19	0.007	0.009		
Control 13 / Target 13	0.52	0.41	0.11	23	0.52	0.41	0.11	23	0.56	0.61	0.47	0.47	0.00	0.09	-23	0.006	0.031		
Control 14 / Target 14	0.43	0.20	0.24	62	0.41	0.30	0.11	57	0.33	0.40	0.35	0.36	-0.02	-0.03	4	0.013	0.026		
Control 15 Target 15	1.48	0.25	1.23	19	0.38	0.29	0.10	14	0.38	0.36	0.48	0.35	-0.10	0.04	22	0.009	0.028		
Control 16 / Target 16	0.47	0.32	0.14	68	0.47	0.36	0.10	64	0.41	0.39	0.42	0.42	-0.01	-0.01	-5	0.010	0.022		
Control 17 / Target 17	0.49	0.29	0.20	22	0.49	0.29	0.20	22	0.36	0.30	0.39	0.39	-0.03	-0.03	-18	0.011	0.044		
Control 18 Target 18	0.39	0.34	0.35	21	0.53	0.21	0.18	22	0.33	0.41	0.31	0.32	0.03	0.01	-18	0.005	0.050		
Control 19 / Target 19	0.54	0.31	0.24	23	0.54	0.37	0.18	22	0.49	0.43	0.46	0.47	0.02	0.02	20	0.006	0.048		
Control 20 / Target 20	0.53	0.34	0.19	55	0.39	0.42	0.11	53	0.44	0.42	0.48	0.49	-0.05	-0.05	1	0.013	0.025		
Plot 1	0.44	0.05	0.38	173	0.44	0.22	0.21	160	0.24	0.19	0.34	0.35	-0.10	-0.11	-10			0.21	0.13
Plot 2	0.46	0.19	0.38	293	0.44	0.19	0.27	276	0.28	0.47	0.38	0.39	-0.10	-0.11	-4			0.42	0.27

Plot 3	0.32	-0.19	0.51	264	0.29	0.11	0.18	246	0.13	0.31	0.20	0.21	-0.07	-0.08	8			0.23	0.22
Plot 4	0.31	0.03	0.28	166	0.31	0.14	0.18	157	0.20	0.35	0.24	0.24	-0.03	-0.04	15			0.59	0.32
Plot 5	0.40	0.01	0.40	163	0.40	0.19	0.21	150	0.39	0.44	0.31	0.32	0.08	0.07	15			0.28	0.19
Plot 6	0.39	-0.01	0.39	187	0.39	0.07	0.32	179	0.32	0.38	0.30	0.30	0.03	0.02	-10			0.34	0.23
Plot 7	0.42	0.16	0.26	173	0.42	0.02	0.39	156	0.35	0.42	0.30	0.31	0.05	0.04	-14			0.3	0.24
Plot 8	0.51	0.21	0.31	144	0.51	0.27	0.25	139	0.41	0.52	0.38	0.39	0.03	0.02	-24			0.25	0.18
Plot 9	0.40	-0.05	0.45	111	0.40	0.09	0.31	107	0.28	0.36	0.28	0.28	0.00	0.00	-18			0.29	0.21
Plot 10	0.60	0.29	0.31	173	0.60	0.29	0.31	169	0.39	0.68	0.47	0.47	-0.09	-0.09	-15			0.8	0.55

Bare Soil 1 * Area 1 m^2	0.557	0.168	0.389		0.53	0.373	0.157		0.40		0.427	0.434	0.281	0.287					
Bare Soil 2 * Area 1 m^2	0.557	0.168	0.389		0.53	0.373	0.157		0.40		0.453	0.461	-0.050	-0.058					
Bare Soil 3 * Area 1 m^2	0.541	0.232	0.31		0.541	0.39	0.151		0.43		0.462	0.470	-0.034	-0.042					
Bare Soil 4 * Area 1 m^2	0.528	0.013	0.515		0.528	0.351	0.177		0.42		0.430	0.444	-0.010	-0.024					
Bare Soil 5 * Area 1m^2	0.568	0.062	0.506		0.556	0.394	0.162		0.41		0.467	0.478	-0.061	-0.072					
Bare Soil 6 * Area 0.5 m^2	0.527	0.309	0.22		0.527	0.407	0.12		0.40		0.455	0.463	-0.052	-0.060					

6.9 Comparison of data exported with the two different methodologies

Plot 1					
x / ArcGIS	x / Las2txt	y / ArcGIS	y / Las2txt	z / ArcGIS	z / Las2txt
300698.6	300698.6	5039301.2	5039301.2	0.05	0.05
300699.1	300699.1	5039301.2	5039301.2	0.10	0.10
300699.3	300699.3	5039301.5	5039301.5	0.10	0.10
300699.1	300699.1	5039301.6	5039301.6	0.13	0.13
300698.8	300698.8	5039301.1	5039301.1	0.14	0.14
300698.3	300698.3	5039301.5	5039301.5	0.15	0.15
300698.9	300698.9	5039301.7	5039301.7	0.16	0.16
300698.5	300698.5	5039301.7	5039301.7	0.18	0.18
300698.6	300698.6	5039301.1	5039301.1	0.19	0.19
300698.7	300698.7	5039301.8	5039301.8	0.19	0.19
300698.7	300698.7	5039300.8	5039300.8	0.19	0.19

6.10 Part of the data extracted in the area referred as bare soil 1 and the calculations made with this data

N°	Bare Soil 1 - Z (m)				
	All the points	Outlier	Zmax/With Outliers (m)	Zmin/With Outliers (m)	Cloud Thickness/With Outliers (m)
1	0.091	Yes/Inf	0.519	0.091	0.43
2	0.191	Yes/Inf			
3	0.203	Yes/Inf			
4	0.220	Yes/Inf	Zmax/Without Outlier (m)	Zmin/Without Outlier (m)	Cloud Thickness/Without Outlier (m)
5	0.276	Yes/Inf	0.519	0.313	0.21
6	0.295	Yes/Inf			
7	0.299	Yes/Inf			
8	0.313	No	GPS Point Z (m)	Average Z/ With Outliers (m)	Average Z/ Without Outliers (m)
9	0.314	No	0.384	0.427	0.434
10	0.314	No			
11	0.315	No		Z Variation/With Outliers (m)	Z Variation/ Without Outliers (m)
12	0.322	No		-0.043	-0.050
13	0.325	No			
14	0.326	No			
15	0.334	No			
16	0.336	No			
17	0.345	No			
18	0.352	No			
19	0.354	No			
20	0.356	No			
21	0.373	No			
22	0.375	No			

6.11 Part of the data extracted in the area referred as control 1 and the calculations made with this data.

N°	Control 1 - Z (m) - Ground Control Points Archetipo Area 50x50cm											
	All the points / LiDAR	Outlier	Classification/Arcgis	x	y	Scan Angle	DSM z	DSM x	DSM y	Zmax/With Outliers (m)	Zmin/With Outliers (m)	Cloud Thickness (m)/With Outliers
1	-0.020	Yes/Inf	Ground	300665.4	5039221.3	4	0.380	300665.5	5039221.2	0.492	-0.020	0.51
2	0.403	No	Other	300665.4	5039221.3	4	0.380	300665.5	5039221.2	Zmax/Without Outlier (m)	Zmin/Without Outlier (m)	Cloud Thickness/Without Outlier (m)
3	0.372	No	Other	300665.4	5039221.3	9	0.381	300665.5	5039221.3	0.492	0.341	0.15
4	0.443	No	Other	300665.5	5039221.1	8	0.381	300665.6	5039221.2	GNSS Point Z	Average Z/ With Outliers (m)	Average Z/ Without Outliers (m)
5	0.426	No	Other	300665.2	5039221.1	6	0.381	300665.6	5039221.2	0.351	0.400	0.410
6	0.462	No	Other	300665.3	5039221.2	6	0.381	300665.5	5039221.2		Z Variation/With Outliers (m)	Z Variation/ Without Outliers (m)
7	0.417	No	Other	300665.3	5039221.2	5	0.381	300665.6	5039221.3		-0.049	-0.059
8	0.426	No	Other	300665.3	5039221.4	6	0.381	300665.5	5039221.3	Point Count LiDAR/ Without Outliers	Point Count LiDAR/ With Outliers	Average Z / DSM
9	0.364	No	Other	300665.5	5039221.4	6	0.381	300665.5	5039221.2	40	41	0.394
10	0.377	No	Other	300665.5	5039221.3	7	0.381	300665.6	5039221.2	Average Scan Angle	Standand Deviation / Lidar	Standand Deviation / DSM
11	0.439	No	Other	300665.3	5039221.1	7	0.381	300665.5	5039221.2	7	0.036	0.010
12	0.380	No	Other	300665.4	5039221.3	7	0.381	300665.5	5039221.3			
13	0.379	No	Other	300665.5	5039221.2	7	0.381	300665.6	5039221.2			
14	0.429	No	Other	300665.5	5039221.4	7	0.381	300665.6	5039221.2			
15	0.430	No	Other	300665.5	5039221.2	7	0.381	300665.6	5039221.3			
16	0.381	No	Other	300665.5	5039221.3	6	0.381	300665.5	5039221.2			
17	0.346	No	Other	300665.5	5039221.3	7	0.381	300665.6	5039221.3			
18	0.414	No	Other	300665.5	5039221.1	6	0.381	300665.5	5039221.2			
19	0.407	No	Other	300665.4	5039221.3	6	0.381	300665.6	5039221.2			
20	0.370	No	Other	300665.6	5039221.3	8	0.381	300665.5	5039221.3			
21	0.426	No	Other	300665.6	5039221.2	5	0.381	300665.5	5039221.3			

6.12 Part of the data extracted in plot 1 and the calculations made with this data.

N°	Plot1 - Z (m)									
	Points/ Lidar Cloud	Classification/Arc Gis	Outlier	ScanAngle	x	y	GNSS Points	Zmax/With Outliers	Zmin/With Outliers	Cloud Thickness (m)/With Outliers
1	0.054	Ground	Yes/Inf	-9	300698.6	5039301.2	0.252	0.436	0.054	0.382
2	0.096	Ground	Yes/Inf	-9	300699.1	5039301.2	0.222			
3	0.096	Ground	Yes/Inf	-9	300699.3	5039301.5	0.229			
4	0.125	Ground	Yes/Inf	-9	300699.1	5039301.6	0.243	Zmax/Without Outliers	Zmin/Without Outlier	Cloud Thickness/Without Outlier (m)
5	0.141	Ground	Yes/Inf	-9	300698.8	5039301.1	0.244	0.436	0.223	0.213
6	0.153	Ground	Yes/Inf	-9	300698.3	5039301.5				
7	0.162	Ground	Yes/Inf	-9	300698.9	5039301.7				
8	0.184	Ground	Yes/Inf	-9	300698.5	5039301.7		GPS Point Z /Mean	Average Z/ With Outliers	Average Z/ Without Outliers
9	0.186	Ground	Yes/Inf	-9	300698.6	5039301.1		0.238	0.337	0.351
10	0.186	Ground	Yes/Inf	-9	300698.7	5039301.8				
11	0.19	Ground	Yes/Inf	-9	300698.7	5039300.8		Average Scan Angle /Whithout Outliers	Z Variation/With Outliers	Z Variation/ Without Outliers
12	0.227	Ground	Yes/Inf	-9	300698.8	5039301.3		-10	-0.099	-0.113
13	0.262	Ground	No	-9	300698.6	5039301.9		Point Count with Outliers	Point Count without Outliers	
14	0.223	Other	Yes/Inf	-9	300699.0	5039300.0		173	160	
15	0.258	Other	No	-9	300698.0	5039300.0				
16	0.261	Other	No	-9	300699.0	5039300.0				
17	0.266	Other	No	-10	300698.0	5039300.0				
18	0.269	Other	No	-10	300699	5039300				
19	0.272	Other	No	-10	300699	5039300				